Foraminiferal Analysis of Holocene Sea Level Rise within Trinity River Incised Paleo-Valley, Offshore Galveston Bay, Texas

Standring, P.[1,2]*, Lowery, C. [1], Burstein, J. [1,2,^], Swartz, J. [1,2,#], Goff, J. [1,2], Gulick, S.P.S. [1,2]

[1]Institute for Geophysics, University of Texas at Austin, Texas

[2]Department of Geological Sciences, University of Texas at Austin, Austin, Texas

*Corresponding Author: patty.standring@utexas.edu

[#]Now at: Water Institute of the Gulf, Baton Rouge, Louisiana

[^]Now at: T. Baker Smith, LLC, Aransas Pass, Texas

Highlights:

- Micropaleontology as environmental context for seismic and sedimentologic analysis
- Long-term (~2 kyr) stable estuary amid early Holocene sea-level rise
- Revised paleoshoreline model matching characteristic geometry of modern shoreline

Abstract

Sea-level is expected to continue to rise in the next century, and as society prepares to deal with this hazard it is critically important to understand how coastal systems will respond, especially in regions with rapid rates of coastal erosion and relative sea-level rise like the Gulf of Mexico Texas coast. Tide gauge records in Galveston Bay, Texas, indicate that local sea level rise rates are more than twice the global average, raising important questions about the long-term stability of the barrier islands protecting the bay and how the estuary and coastline will respond to sea-level rise. However, tide gauge records only go back to the beginning of the last century, and longer records are needed to provide insight into dynamic coastal response to sea-level fluctuations. Here, we combine geophysical (chirp sub-bottom profiler) surveys and sediment cores (providing sedimentological and micropaleontological data constrained by radiocarbon dating) to characterize paleoenvironmental change in the Holocene estuary system offshore modern Galveston Bay over the last ~10 kyr; with the first 4 kyr of this time span undergoing a period of rapid sea level rise more than twice the modern rate. Our foraminiferal analysis provides ecological context on the stability of these paleoenvironments and the timing of coastal change over the last ~10 kyr. We provide a model of Holocene shoreline change differing from existing interpretations of rapid landward shifts with asymmetric coastal geometry to one composed of more gradual transitions matching modern coastal geometry and argue for an overall stable paleoestuarine environment throughout the middle Holocene (~6.9 ka – 8.8 ka).

Subsequent shoreline shifts occurred after global sea level rise slowed below modern rates, indicating hydroclimate impacts on sediment flux likely had a greater influence on the earlier stability of the estuarine system and later shoreline retreat than rates of sea-level rise.

Keywords: Sea level change, micropaleontology (forams), N America

1. Introduction

As global sea levels continue to rise, constraining how coastlines respond is increasingly important for coastal planning. High estimates of sea-level rise exceed 2 m above current mean levels by 2100 for +5°C of warming, in which CO_2 emissions are not curbed, while lower estimates for +2°C of warming, which falls in line with plans that cut CO_2 emissions globally, put sea-level rise at 0.26-0.81 m by 2100 (Bamber et al., 2019). Even this lower range of sea level rise presents a significant threat to coastal communities (Bamber et al., 2019; Bernstein et al., 2019) which represent ~10% of the world's population (FitzGerald et al., 2008). A 1.8 m rise in sea level would inundate six million coastal homes in the U.S. and risks one trillion dollars in damage to coastal residential real estate (Bernstein et al., 2019). Global mean sea-level rise does not impact areas equally and some areas will experience significantly higher flooding rates over the next century (Vitousek et al., 2017); thus, it is important to understand regional and local coastal response to rising seas.

Low-gradient, low-elevation coastlines around the Gulf of Mexico are especially vulnerable to the destruction caused by large storms and hurricanes, requiring significant periods of time for barrier island systems to adjust and recover (Bernstein et al., 2019; FitzGerald et al., 2008; Goff et al., 2010; Palermo et al., 2021; Shawler et al., 2021). Industrial development, dredging for navigation purposes in the back-barrier, reduction of natural wetlands, and increased subsidence due to extraction of hydrocarbons and groundwater contribute to the Gulf Coast's vulnerability to sea level rise and coastal inundation, particularly in areas like Galveston Bay (Anderson et al., 2008; Kirwan and Megonigal, 2013; Paine, 1993; Shawler et al., 2021; White et al., 2002). Despite recent local regulations concerning groundwater extractions, compaction and subsidence from 20th century pumping is estimated to continue over several hundred years (Miller and Shirzaei, 2021). As the busiest shipping center in the U.S. (Port of Houston, 2021), Galveston Bay represents a particular vulnerability of U.S. supply chains and infrastructure due to sea level inundation. As a result of heavy development, the western boundary of Galveston Bay no longer consists of protective wetlands (Anderson et al., 2008) and overall wetland loss in the Trinity River delta area exists due to subsidence and relative sea level rise (White et al., 2002). Barrier islands, like those that enclose Galveston Bay, evolve due to sea-level rise on centennial to millennial timescales, and sediment transport along the shoreline, with local-scale conditions altering the timing of barrier erosion and progradation processes (Fruergaard et al., 2015; Lentz et al., 2013; Raff et al., 2018; Shawler et al., 2021). These processes are also highly influenced by antecedent topography and slope, and sediment supply within the substrate, where muddier substrates result in barriers that are prone to collapse and drowning, and shallower slopes will experience more rapid drowning and disintegration of barrier systems than steeper slopes under the same rate of sea-level rise (Brenner et al., 2015; Lorenzo-Trueba and Ashton, 2014; Moore et al., 2010; Raff et al., 2018; Shawler et al., 2021). In general, shallower back-barrier environments experience more rapid landward migration of barrier islands (Lorenzo-Trueba and Ashton, 2014; Moore et al., 2010; Shawler et al., 2021). As back-barrier marshes and coastal wetlands are inundated and converted to intertidal and subtidal environments, the tidal prism of the bay is enlarged, which increases the volume of sand contributed to ebb- and flood-tidal deltas (Al Mukaimi et al., 2018; FitzGerald et al., 2008). This process leads to the denudation of barrier systems, furthering the erosion of coastal environments (FitzGerald et al., 2008).

Understanding how specific areas of the Gulf Coast have responded to relative sea level rise in the past provides predictions for future coastal vulnerabilities, especially in populated areas that are undergoing rapid coastal land loss, like Galveston Bay, Texas (Anderson et al., 2016, 2008; Phillips et al., 2004; White et al., 2002). Flood hazard assessments predict over 76 km^2 along the Texas coast will subside below sea level by 2100, which alone increases the area of inundation due to sea-level rise by 39% (Miller and Shirzaei, 2021). Subsidence within Galveston Bay is lowest near the mouth of the San Jacinto River and the Houston Ship Channel, and although sedimentation rates are higher in this area than the rest of Galveston Bay, they are almost 50% lower than rates of sea-level rise generating an accretionary deficit (Al Mukaimi et al., 2018).

Instrumental records help identify trends in sea level changes along the coasts, while highlighting specific coastal regions at increased risk of land loss. Monthly mean sea level measurements at Galveston Bay Pier 21 establish relative sea-level rise trends with a 95% confidence level of $+6.59 \pm 0.22$ mm yr^{-1} over the time period from 1904-2020, and at $+6.62 \pm 0.69$ mm yr^{-1} from 1957-2011 for Galveston Pleasure Pier (NOAA, 2021). This rate is significantly higher than all other stations along the Texas Coast, and even double in some cases. For example, Padre Island data show a sea-level rising trend of $+3.48 \pm 0.75$ mm yr^{-1} from 1958-2006, and $+3.54 \pm 0.70$ mm yr^{-1} at Port Mansfield, Texas, from 1963-2020 (NOAA, 2021). Nearby Sabine Pass, Texas, shows a similar, but lower, trend of +6.16 ± 0.74 mm yr^{-1} from 1958-2020 (NOAA, 2021). Observations of coastal erosion by the Texas Bureau of Economic Geology show a net retreat of 1.24 m yr^{-1} for the entire Texas coast, and a rate of 0.4 m yr^{-1} for Galveston County on the western side of Galveston Bay, and 1.63 m yr^{-1} for Chambers County on the eastern side of Galveston Bay (Paine et al., 2011). The report specifically highlighted the area of sandy beach west of the seawall on Galveston Island as undergoing significant shoreline retreat, whereas longshore current causes net shoreline advance on Bolivar Peninsula east of the Bolivar Roads tidal inlet, which is likely due to the construction of jetties on either side of the inlet (Paine et al., 2011).

Unfortunately, instrumental data are limited by the short timescales they cover, on the Gulf Coast only going as far back as the early 1900s (and more commonly several decades later). These instrument records often start after accelerated sea-level rise has been initiated, introducing a potential bias in future rising sea level predictions and modeling (Horton et al., 2019). Therefore, it is necessary to use the geologic record to augment the instrumental data and determine how past coastal changes have been influenced by accelerated sea level rise (Horton et al., 2019).

Looking further back in time provides insight into the impact of rapid sea level rise on coastlines (Dutton et al., 2015; Horton et al., 2019). As part of a Bureau of Ocean Energy Management funded effort to identify subsurface sand resources along the Gulf shelf for coastal resilience and nourishment projects, the Trinity River Incised Paleo-Valley Project has conducted multiple seismic surveys and sediment coring to map the Trinity River-incised valley offshore modern Galveston Bay and chart its transformation from a Pleistocene fluvial to Holocene estuarine to modern open marine environment. Here, we use high-resolution seismic data in combination with micropaleontological analysis, sedimentology, carbon dating, and age modeling from sediment cores to develop a comprehensive history of Holocene paleoenvironmental and coastal change in the Trinity paleo-valley over the last 10 kyr, during which time sea level rise slowed from 5 mm yr^{-1} to 3 mm yr^{-1} (Milliken et al., 2008). We identify periods of estuary stability through barrier island development and subsequent shoreline retreat.

2. Regional Setting/Background

Modern Galveston Bay is located on the northeast Texas coast in the Gulf of Mexico and consists of multiple bays that comprise the Estuary Complex (Figure 1). The microtidal, wave-dominated regime in the Gulf of Mexico allows for long, narrow, relatively straight barrier island system protecting the estuary, consisting of Bolivar Peninsula on the eastern side of the bay and Galveston Island on the western side (Anderson et al., 2016, 2014; Davis and Hayes, 1984; FitzGerald et al., 2008; Rodriguez et al., 2004). The shape of Galveston Bay developed when existing fluvial topography was inundated as the bay mouth was restricted to a tidal inlet ~2.5 ka (Anderson et al., 2016, 2008; Rodriguez et al., 2004). Construction of jetties has restricted sediment flow through Bolivar Roads, the primary inlet into the estuary (Anderson et al., 2008; Siringan and Anderson, 1993).

John Anderson and his research group at Rice University established a firm foundation of research on modern Galveston Bay and its transformation throughout the Holocene (Anderson et al., 2016, 2014, 2008; Milliken et al., 2008; Rodriguez et al., 2005, 2004; Simms et al., 2007; Siringan and Anderson, 1993). During Marine Isotope Stages (MIS) 5-3, the region experienced episodic sea-level fall, which led to the creation of Trinity and San Jacinto incised river valley (Figure 2 & 3) (Anderson et al., 2016, 2014; Swartz, 2019). Stepped downcutting throughout the incised valley resulted in terraced morphology (Anderson et al., 2016, 2008; Rodriguez et al., 2005). The upper, wider portions of the incised valley are not visible in the sediment record because they have been removed by shoreface erosion to the transgressive ravinement during Holocene sea-level rise, identified at -8 to -10 m depth along the Texas coast as the onlapping of marine muds onto a “decapitated shoreface” (Anderson et al., 2016; Rodriguez et al., 2004).

Global sea-level rise between ~11.4 and 8.2 ka is estimated at ~15 m kyr^{-1} followed by a reduced rate of sea-level rise 8.2-6.7 ka, coinciding with the final deglaciation of North America (Lambeck et al., 2014). Along the Gulf Coast, sea level began to rise episodically between ~10 and 7 ka, after which it slowed to steady present day levels (Figure 2) (Anderson et al., 2016, 2014; Milliken et al., 2008; Swartz, 2019). The Anderson group identified multiple flooding surfaces within the Trinity incised valley that occur either contemporaneously with other areas along the Gulf coast and are attributed to rapid sea-level rise, or exist locally, suggesting forcing mechanisms such as changing sediment supply and/or antecedent topography (Anderson et al., 2016; Rodriguez et al., 2005). Radiocarbon dating in sediment cores from modern Galveston Bay constrain rapid sea-level rise events to 9.6 ka, 8.2 ka, and between 7.7 and 7.4 ka, in which each inundation was complete after only a few centuries (Figure 4) (Anderson et al., 2008). Milliken et al., (2008) identified flooding events consistent with radiocarbon dates and relative sea level changes within the Gulf of Mexico at 9.5-9.8 ka, 8.5-8.9 ka, 8.0-8.4 ka, and 6.8-7.4 ka (Figure 2).

Estimates of Antarctic ice-sheet fluctuations since the Last Glacial Maximum vary widely, so most Holocene sea-level rise is attributed to the better constrained demise of the Laurentide Ice Sheet (LIS), with some evidence for Antarctic melting after ~6 ka (Lambeck et al., 2014). Higher resolution analysis of LIS deglaciation reveals multiple meltwater pulses at 9.1 ka, 8.7 ka, 8.6 ka, and 8.2 ka, and 7.4 ka (Jennings et al., 2015). After 8.15 ka, LIS retreat accelerated with remnant ice domes melting by ~6.7 ka (Lambeck et al., 2014; Ullman et al., 2016). Remaining global sea-level rise is attributed to the loss of ice volume from the West Antarctic ice-sheet during the late Holocene (Ullman et al., 2016).

Approximately 9.6 ka, the initial inundation of modern Galveston Bay shifted the upper bay ~30 km up the incised valley, coincident with LIS retreat and Hudson Strait freshwater drainage (Anderson et al., 2008; Jennings et al., 2015; Lambeck et al., 2014; Thomas and Anderson, 1994). The early opening of the Tyrell Sea ~8.6 ka and the catastrophic release of freshwater from North American glacial lakes occurred at 8.15 ka (Jennings et al., 2015). At the same time the bayhead delta shifted ~10 km up the valley, partially attributed to a “dramatic decrease in sedimentation rates” from 4.6 mm yr^{-1} to 1.3 mm yr^{-1} and the coincident elevation of a Pleistocene-age terrace (Figure 4) (Anderson et al., 2008). Higher temperatures in the Atlantic Meridional Overturning Circulation, likely due to Antarctic ice sheet loss, and strengthening of the North Atlantic Deep Water led to a warming period 7.9 ka (Cronin et al., 2007) in which remnant ice domes of the LIS were significantly melted (Ullman et al., 2016). Between 7.7 and 7.4 ka the upper bay shifted a further ~25 km up the valley at a rate of 8 km $century^{-1}$ but maintained its existing shoreline ~50 km seaward of the modern coastline, which produced a ~100-km-long paleoestuary (Anderson et al., 2008; Rodriguez et al., 2005). This flooding event occurred despite the decreasing rate of sea-level rise between 7.5 and 7.0 ka, with coincident events in Matagorda Bay and Sabine Lake, and is attributed to a Gulf Coast climate transition from cool and moist to warm and dry, reducing sediment supply (Anderson et al., 2008).

Radiocarbon dating of sandy sediments from Heald Bank suggest that the paleoshoreline was in that location by as late as 7.7 ka, while ages obtained from the oldest beach ridges on Galveston Island constrain its development to 5.5 ka (Figure 1) (Anderson et al., 2014, 2008; Rodriguez et al., 2005, 2004). Conflicting interpretations of Heald Bank sands call into question the 7.7-ka-shoreline, and suggest the bank may be marine in origin, like Thomas and Shepard Banks, and developed after the shoreline had already shifted up-valley (Thomas and Anderson, 1994). Bolivar Peninsula began to develop as a spit ~2.5 ka and as it prograded westward, the tidal inlet narrowed to a fraction of its original size to form Bolivar Roads tidal inlet allowing flooding along the bay boundaries, establishing the modern shape of Galveston Bay (Anderson et al., 2016, 2014, 2008; Rodriguez et al., 2005, 2004).

Although prior sedimentological and seismic research conducted by the Anderson group is thorough, it has thus far lacked sufficient paleoenvironmental evidence and the spatial coverage necessary to establish the evolution of the paleo-estuary (Anderson et al., 2008; Rodriguez et al., 2004). Additional higher resolution seismic data combined with radiocarbon dating of sediment cores and micropaleontological interpretations of facies changes will characterize coastal change by temporally and spatially constraining a large and long-term stable estuarine environment and the transformation of the coastline throughout the Holocene. Foraminifera are powerful proxies for paleoenvironmental and relative sea level change because of their sensitivity to temperature, salinity, and nutrient availability (Culver, 1988; Gehrels, 2013; Olson and Leckie, 2003; Phleger, 1951; Poag, 1981). Modern assemblages represent a specific "physicochemical environment" within ecological niches or biozones that can be translated to fossil assemblages in sediment cores to identify paleoenvironmental changes as a result of relative sea level fluctuations forming a link between instrumental and fossil records (Culver, 1988; Phleger, 1960; Gehrels, 2013; Olson and Leckie, 2003; Phleger, 1965; Poag, 1981). This link allows us to differentiate upper, middle, and outer bay environments within otherwise unremarkable successions of estuarine mud and separate sandy ebb- and flood-tidal delta deposits from back-barrier washover fans. Benthic foraminiferal assemblages provide paleoenvironmental context to seismic data and allow for the clarification of the timing of the inundation of the Trinity River Paleovalley and the interpretation of barrier island stability and rollover rate amid rising sea levels at a higher resolution than has previously been possible.

3. Methods

3.1 *Seismic Data*

Approximately 1,000 km of high-resolution seismic data were obtained during two field courses and two cruises funded by the Bureau of Ocean and Energy Management (BOEM) for the purpose of researching sand deposits. These surveys were conducted with an EdgeTech 512i sub-bottom profiler with 0.7 to 12 kHz frequency sweep, 20 ms pulses by the University of Texas Institute for Geophysics (UTIG) (Figure 1). These data were incorporated with 690 line-km of high-resolution chirp seismic surveys conducted by Texas A&M Galveston and the U.S. Geological Survey (USGS) in 2009 using EdgeTech Geo-Star FSSB system and SB-0512i towfish with 20 ms pulse length and 0.7-12 kHz sweep frequency aboard the R/V Manta

(Dellapenna et al., 2009). Processing of UTIG chirp data and interpretation of seismic horizons were conducted by Swartz (2019) and Burstein et al., 2021. UTIG data include full-waveform processing providing a higher resolution of the subsurface stratigraphy (Goff et al., 2015). Seismic lines corresponding to sediment cores were converted from two-way travel time in milliseconds to meters with an approximate seismic wave velocity of 1525 m s^{-1} (Abdulah et al., 2004).

3.2 *Piston and gravity coring*

Piston core (PC) sites (Figure 1) were chosen based on sedimentary structures observed in seismic data to pinpoint key transitions in the sedimentary record and evaluate paleoenvironmental evolution from fluvial to estuarine to modern-day marine. Piston cores were collected during a cruise of the R/V *Brooks McCall* as part of UTIG's 2018 Marine Geology and Geophysics (MGG) Field Course. Gravity core (GC) locations (Figure 1) were selected during processing to clarify additional points of interest, particularly along the valley edges, and were collected during a BOEM-UTIG cruise of the R/V *Manta* in 2019.

Piston and gravity cores were split onshore after both cruises were completed. The archive halves were stored, and the working halves were described for appearance, visual grain size, bioturbation, and presence of marine fauna (e.g., shell fragments and shell hash), and terrestrial organic material (e.g., plant debris). Sediment samples for microfossil analysis were selected at 10- to 50-cm intervals from piston and gravity cores, and at specific points where a paleoenvironmental transition may have occurred based on changes observed in the core, avoiding sandier sediments. Piston core 2 (PC-2) was the longest core collected and was sampled at higher resolution to serve as a reference section. Subsequent sampling in piston core 4 (PC-4) and all the gravity cores (GC-1 thru GC-6) was done at a lower resolution with additional samples selected to more precisely identify paleoenvironmental transitions. Samples were soaked for at least 24 hours in a mixture of borax and hydrogen peroxide to break down clay floccules, washed over a 63-µm sieve, and dried in an oven.

3.3 *Foraminiferal analysis*

Samples were split to provide a reasonable amount of material and foraminifera were picked using a binocular microscope and placed on a slide. Population sizes of at least 100 foraminifera tests were picked where possible (some samples were barren or did not yield 100 individuals) and identified at the genus level. Foraminifera that were not identifiable at the genus level were classified as “benthic spp.” Confidence interval calculations (see Appendix A) show that these population sizes are sufficient to track changes in predominance facies (i.e., *Ammonia* vs. *Elphidium*) within the estuary. Confidence intervals were based on the binomial method provided in Buzas (1990). Modern grab samples from Bolivar Roads tidal inlet obtained during the MGG 2018 Field Course were analyzed and used as a comparison for flood- and ebb-tidal delta sediments in the cores. Samples were soaked overnight in a 1% solution of Rose Bengal and water immediately after collection to stain specimens which were living or recently living. Samples were then sieved and dried in an oven. Populations of at least 300 individuals were picked and identified at the genus level (see Appendix A).

Predominance facies are defined by genus of foraminifera (Culver, 1988; Poag, 1981). Poag (1981) synthesized analysis of modern benthic foraminiferal assemblages in the Gulf of Mexico

(Figure 5) and outlined predominance facies for Galveston Estuary Complex based on the previous work conducted by Wantland (1969) within the Trinity Bay and written communication from W.V. Sliter of the USGS. Wantland (1969) collected 87 samples from stations within the subaerial Trinity River delta and Trinity Bay and used Rose Bengal solution to determine live taxa at time of collection. Live samples were picked from 62-µm sieved wet sediments and populations were based on at least 300 individual tests where possible (Wantland, 1969). Poag (1981) identified the following modern predominance facies for Galveston Bay: dominance of *Ammotium* represented upper bay or river delta facies, dominance of *Ammonia* indicated central bay facies, and dominance of *Elphidium* was determined to be outer bay facies (Figure 5). Culver (1988) also outlined a priori groups of prominent foraminifera genera by depth and environmental preference, which match well with Poag's predominance facies. Culver (1988) specified genera of foraminifera that can be considered diagnostic of certain environments: *Ammotium* for marshes, *Ammobaculites* and *Elphidium* for bays/estuaries, and *Bolivina* spp., *Bulimina* spp., and *Elphidium* spp. for inner shelf environments (Figure 5).

Paleoenvironmental interpretations of the Holocene estuary system are based off of assemblage percentages of three primary genera outlined by Poag (1981). Samples with >50% *Ammonia* are interpreted as central bay facies, samples with ~50-50 *Ammonia/Elphidium* are transitional to outer bay, and samples with >50% *Elphidium* are outer bay facies. *Ammotium*, indicative of Poag's bayhead delta facies, was typically not identifiable at the genus or species level due to test fragmentation. Agglutinated taxa are generally uncommon and are poorly preserved in our cores, so they were categorized as agglutinated spp. We interpret increases in the presence of agglutinated spp. to indicate proximity to bay margin environments that are more likely to be dominated by agglutinated taxa. An overall increase in diversity including common inner shelf taxa (e.g., *Bulimina*, *Bolivina*, miliolids, etc.) coupled with a resurgence of *Ammonia* spp. likely indicates a transition to modern marine or open shelf facies (Culver, 1988; Olson and Leckie, 2003; Poag, 1981). Facies lacking in foraminifera were deemed barren and, given their stratigraphic position, interpreted to reflect the transition to terrestrial (e.g., fluvial) environments.

Estuaries are dynamic environments and reworking of material is likely common. To identify areas of potential reworking, foraminiferal test fragments (interpreted to be broken during redeposition) within each sample were counted in addition to individual identifiable tests for population totals. Total fragments were normalized to total foraminifera to provide a percent fragmentation for each sample. Peaks in fragmentation are interpreted as potential periods of increased energy or sediment reworking, and in some cases coincided with decreased foram populations.

3.4 *Radiocarbon dating*

Sediment cores were sampled for radiocarbon dating to provide age constraints on paleoenvironmental transitions and develop age models for each core. A total of 28 samples were sent to the National Ocean Sciences Accelerator Mass Spectrometry (NOSAMS) at Woods Hole Oceanographic Institute for radiocarbon dating using the Libby half-life of 5,568 yr and corrected for carbon isotopic fractionation. Of these samples, 23 were mollusk shells, 2 were comprised of foraminiferal tests, and 3 contained organic material/plant debris (Table 1). Mollusk and foraminiferal samples containing at least 4 mg of material underwent hydrolysis where carbon in the samples were converted to CO_2 using a strong acid H_2PO_3. Mollusk samples were powdered to allow NOSAMS staff to subsample material >9 mg. Radiocarbon dates from organic material were calibrated with IntCal20 (Reimer et al., 2020) and mollusk and foraminifera ages were corrected for reservoir variations using a correction specific to the Gulf of Mexico offshore Galveston Bay (Wagner et al., 2009) and then calibrated using Marine20 (Heaton et al., 2020). The IntCal20 calibrations were done via OxCal 4.4 (Ramsey, 2009) and the Marine20 calibrations were applied through Bchron (Haslett and Parnell, 2008). Errors in ages were calculated by NOSAMS where the error is determined by the larger of two estimates, the internal statistical error calculated using the total number of ^{14}C counts (error = $1/\sqrt{n}$) and the external error determined by the ratio of ^{14}C and ^{12}C of a sample calculated 10 separate times while the sample was being run.

3.5 *Age models*

Age models were developed using the code rbacon (Blaauw and Christen, 2011), which calculates sediment accumulation rates based on a gamma autoregressive semiparametric model using a Markhov chain Monte Carlo algorithm. The model provides a predictive window with 95% confidence of the age of sediments given depth and radiocarbon age constraints and the assumption of consistent deposition unless hiatuses are applied. Although we suspect a significant amount of erosion may have occurred during transgression, the lack of upper core carbon dates limits the application of hiatus depths in the model and interpolated ages for the upper core are likely incorrect. Interpolated ages from the models for each core (except for GC-1) were used to identify environmental transitions between radiocarbon ages, and in a few instances, extrapolated ages were used to identify transitions outside the range of carbon dates.

4. Results

Sediment cores range from <1 m to ~ 5.6 m in depth and primarily contain medium-gray mud varying from clay to silty-clay with sandy intervals that occasionally coincide with shell hash layers or abundant shell fragments (Figure 6). GC-4 contains significantly more organic material and less shell material than all the other cores. GC-1 and PC-4 contain sharp and gradual contacts, respectively, between stiff, light-gray Pleistocene clay terraces and Holocene sediments (Figure 6h & 6b). PC-2 and PC-4 did not contain any analyzable upper seafloor sediments due to coring disturbance caused by over-penetration of the piston corer and the soupy nature of the uppermost sediments. Here, we summarize the key observations for each core, proceeding from the most proximal to most distal core.

4.1 *Piston core 2*

PC-2 was selected for identification of a fluvial terrace toward the western edge of the incised valley (Figure 7A). It consists primarily of massive medium-gray clay with sporadic sandy layers that coincide with increased shell fragments and in some cases shell hash layers (Figure 7). The core catcher contains silty medium sand which is overlain by silt and clay (Figure 6a). As the reference section representing the complete transition from fluvial to outer bay deposition, this core was sampled at the highest resolution at least every 10 cm. The base of the core is barren of foraminifera and is interpreted as fluvial deposits, which are capped by upper bay/deltaic deposits dominated by agglutinated benthics and dated to 9,794 ± 215 cal yr B.P. from a mollusk shell at 5.10 m depth (Figure 7B). The increase in percentage of fragmented foraminifera tests represents a higher energy environment with potentially more reworked material (Figure 7B).

Upper bay deposits transition at ~9.5 ka upward into ~2.8 m of central bay sediments that are generally dominated by *Ammonia* with some increases in presence of *Elphidium*. The age model of this core (Figure 7B) indicates that this central estuary assemblage existed from at least 9.5 to 8.0 ka, indicating a long period of stability in the estuary system during this time. By 7,800 ± 134 cal yr B.P. (mollusk shell at 1.82 m), the environment had transitioned to outer bay, with a foraminiferal assemblage dominated by *Elphidium*. The uppermost meter of the core was not analyzed due to coring disturbance.

4.2 *Piston core 4*

PC-4 was obtained at the location of another fluvial terrace originally interpreted seismically to be a point bar (Figure 8A), but which was instead revealed to be a Pleistocene flood plain deposit comprised of light-gray, stiff Beaumont Clay, into which the MIS5-3 river valley was incised. The terrace is heavily laminated with oxidized sand layers and contains a calcareous nodule, which are relatively common in the Beaumont (Rehkemper, 1969). The terrace gradually transitions upward into heavily burrowed sand (Figure 6b), and both the terrace and the overlying sandy section are barren of microfossils and interpreted as fluvial/terrestrial sediments. At approximately 3.5 m depth, foraminiferal assemblages appear in the sandy sediments and indicate a transition to an upper bay environment, dated to 9,131 ± 158 cal yr B.P. (mollusk shell at 3.44 m) (Figure 8B). These sediments also contain visible burrows and a higher percentage of fragmented foraminifera tests. PC-4 contains less central bay sediments compared to PC-2, likely due to the elevation of the Pleistocene terrace. The seismic data show draping of sediments above and over the terrace (Figure 8A). Central bay sediments were dominated by *Ammonia* and dated to 8,815 ± 175 cal yr B.P. by a mollusk shell at 2.66 m depth. At approximately 2 m depth, *Elphidium* becomes more dominant and the environment transitions to outer bay sediments. According to the age model for this core (Figure 8B), the central bay to outer bay transition occurred ~8.0 ka, coinciding with the same transition in PC-2. The increase in diversity of foraminifera at ~1.30 m depth (e.g., increase in common inner shelf genera, like *Bulimina* and *Bolivina*, and agglutinated taxa) indicate the beginning of a transition to open marine/inner shelf sediments. This section contains two carbon dates at approximately the same depth (1.59 m) from mollusk shells, one of which likely contains reworked material because it records an unreasonable age for sediments filling a Holocene estuary (41,030 ± 1,703 cal yrs B.P.). The other date provides an age of 7,787 ± 136 cal yr B.P. for the outer bay sediments. The upper 1 m section of PC-4 also consisted of material not suitable for sampling likely containing unconsolidated, unstratified inner shelf deposits that became mixed during retrieval. While fragmentation of tests appears low throughout the core, there is a slight increase in the number of fragments in the outer bay section of the core, indicating a higher energy environment.

4.3 *Gravity core 6*

Along the eastern edge of the paleovalley, GC-6 penetrated bright seismic reflectors that are represented in the core as a ~0.8 m sandy package of sediments atop medium-gray estuarine sediments (Figure 9A). Starting at the base of GC-6, clay sediments are dominated by *Ammonia*, indicating a central bay environment dated to 8,367 ± 181 Cal yrs B.P. (mollusk at ~2.1 m depth). These central bay sediments transition to outer bay, as indicated by an increase in *Elphidium* at ~1.7 m depth, with an approximate age of 8.2 ka based on the age model (Figure 9B). Smaller sandy intervals at the top of the outer bay sediments provide mollusk carbon dates of 7,709 ± 147 Cal yr B.P. and 7,760 ± 142 Cal yr B.P. preceding an irregular contact with the sandy package of sediments (Figure 9B). Shell fragments decrease in abundance going up the core, while foraminifer test fragmentation increases going up the core, potentially indicating that the sandy package contains reworked material. A mollusk shell within the sandy package was dated to 4,319 ± 165 Cal yrs B.P. and foraminifera within the sandy package indicate a transition from outer bay to inner shelf was taking place until the uppermost sample (GC-6 7-8.5). This uppermost sample contained a foram assemblage that did not match any other assemblages in the study area. It was compared to modern foraminifera assemblages obtained by Phleger (1965) from Galveston Lagoon on Galveston Island, and two grab samples taken from within the flood- and ebb-tidal areas of Bolivar Roads tidal inlet by the MGG 2018 Field Course (Figure 10, Appendix A). A similar method of foram assemblage comparison was used by Hawkes and Horton (2012) to identify inner shelf-sourced washover sediments from Hurricane Ike on Galveston and San Luis Islands. Our GC-6 comparison revealed that the uppermost sample most closely resembles Phleger's Station 11 sample from Galveston Lagoon (Figure 10). However, the sample does not contain a higher amount of plant debris as would be expected in a back-barrier marsh environment. As a result, the lower portion of the sandy package is interpreted as transgressive lag capped by probable washover deposits, rather than a relict drowned barrier island.

4.4 *Gravity cores 4 and 5*

GC-4 and GC-5 represent a composite section sampling two different seismic facies along the same seismic line, both of which contain central bay sediments (Figure 11 & 12). GC-4, which penetrates the older seismic facies, is unique in that it contains the lowest populations of foraminifera of all the cores. All samples obtained from GC-4 contain less than 100 individuals, and sections of the core are barren of foraminifera (Figure 11B). Situated on the western edge of the paleovalley (Figure 11A), GC-4 primarily consists of medium-gray clay with a relatively higher amount of organic material (Figure 6d), lower amount of shell fragments, and more visible burrowing. The base of the core contains a barren section, which is interpreted as bay margin deposits, and organic material at 3.35 m depth was dated to 8,470 ± 144 cal yr B.P. These deposits transition to central bay sediments dominated by *Ammonia* and *Elphidium* with decreased organic material and increased burrowing and shell fragments (Figure 11B). The age model for this core (Figure 11B) indicates the transition took place ~8.3 ka. Above the central bay sediments, the core transitions back to barren deposits characterized by burrows and organic material at 0.82 m depth dated to 7,977 ± 221 cal yr B.P. and the age model dates the transition at ~1.4 m depth to ~8.1 ka. The upper section of the core contains a thin sand interval with organic material at 0.56 m dated to 7,913 ± 255 cal yrs B.P. and is capped by a section of silty sediments. The foraminiferal assemblage in this section is dominated by *Ammonia* and *Elphidium* with a slight increase in agglutinated and common inner shelf taxa indicating a transition to outer bay and then inner shelf deposits.

GC-5, which penetrated the younger seismic facies in this two-core composite section, contains central bay sediments capped by outer bay deposits (Figure 12). The base of GC-5 contains medium-gray clay with shell fragments, and a single burrow (Figure 6e). Shell material in this section (2.92 m depth) was dated to 8,467 ± 130 cal yr B.P. and foraminifera are dominated by *Ammonia*. The age model (Figure 12B) indicates the central bay to outer bay transition occurred ~8.4 ka. The outer bay sediments are comprised of medium-gray clay containing sporadic 2-4 cm-scale sandy layers that thicken toward the top of the core to decimeter scale layers with more shell fragments. The upper portion of the core also contains a peak in foram fragmentation and is dominated by *Elphidium*. Increasing diversity and presence of agglutinated forams from 1.0 m depth to the top of the core indicate an outer bay depositional environment transitioning to modern day marine inner shelf. The peak in fragmentation at approximately 1.0 m depth coincides with a peak in dominance of *Ammonia* and suggests that the increase in *Ammonia* likely represents reworked material. The outer bay section was dated to 8,445 ± 135 cal yr B.P. at 2.50 m depth and 6,661 ± 169 cal yr B.P. near the top at 0.73 m depth.

4.5 *Gravity core 1*

GC-1 is an extremely short (0.35 m) core (Figure 6h). Its location was selected to investigate dipping reflectors seen in seismic data hypothesized to be a Holocene-aged point bar deposit from a tributary at the edge of the Trinity Paleovalley (Figure 13). Instead, the core penetrated a Pleistocene-age terrace containing sticky, dense, burrowed Beaumont Clay. This clay is capped by burrowed sand and thick shell hash and has a sharp contact with modern inner shelf deposits at approximately 0.14 m depth (Figure 13B). Foraminiferal analysis revealed a large population of foraminifera, dominated by *Elphidium,* within one of the burrows of the terrace. Carbon dating of these foraminifera tests revealed an age of 38,081 ± 1,833 cal yr B.P. almost certainly owing to the inclusion of older material, potentially in the form of dissolved inorganic carbon from the Beaumont Formation. Samples at the terrace contact contained lower populations of foraminifera dominated by *Ammonia.* Sediments above the terrace were dominated by both *Elphidium* and *Ammonia* with a slight increase in agglutinated forams and a more significant increase in inner shelf genera, indicating a transition to a modern marine environment. Two radiocarbon ages were obtained from approximately the same interval in the core (0.05 m depth) as a method of comparing ages from foraminifera tests and mollusk shells. The foraminifera provided an older age of 1,753 ± 143 cal yr B.P. than the mollusk shell, which was dated to 589 ± 97 cal yr B.P. The difference in the ages may indicate an amalgamation of material in a condensed section on the sediment-starved modern shelf, the presence of sediments containing detrital carbonate within the foram tests resulting in an older age, or perhaps diagenetic alteration of the foram tests, with recrystallization of pore water carbonate incorporating older material on the foraminifer tests, which have a higher surface to mass ratio than the mollusk shells. Regardless, both ages indicate a much younger age for the 14 cm thick open shelf deposit (Figure 13B) than any of the estuary sediments in the river valley. A spike in fragmentation of foram tests coincides with the contact between the terrace and modern deposition, indicating a more significant amount of reworking at the contact. Seismic data at this location show prominent draping of sediments along the edges of the terrace (Figure 13A).

4.6 *Gravity core 2*

GC-2's location was chosen to identify a set of dipping reflectors believed to be part of a paleo-tidal-delta (Figure 14A). The core consists primarily of medium-gray clay with numerous layers of silty sand (Figure 6f). The lower part of the core contains foraminifera approximating 50-50 *Ammonia* and *Elphidium*. This assemblage combined with the increased sand content and the relatively higher percent of foram test fragmentation indicate this section likely contains tidal delta deposits. Because it is capped by a less-sandy section dominated by *Elphidium* indicating an outer bay environment, the base of the core is interpreted as a flood-tidal delta. Carbon dates obtained near the transition from tidal delta to outer bay provide ages of 8,445 ± 135 cal yr B.P. from a mollusk shell at 2.07 m depth and 8,546 ± 173 cal yr B.P. also from a mollusk shell at

2.19 m depth. The top of the core contains a spike in *Ammonia* coupled with an increase in fragmentation. Similar to GC-5, coincident increase in fragmentation with a spike in *Ammonia* likely represent a reworking of central bay material in the outer bay environment. The top of the core contains a transition to modern inner shelf deposition at ~7.0 ka, represented by the increase in diversity and presence of agglutinated foraminifera at ~0.5 m depth.

5. Discussion

The coring locations in this study were chosen to sample specific seismic facies and were not intended to provide a cross-section down the Holocene estuary. However, the data can provide several short cross sections along strike in the proximal, middle, and distal parts of our study area. Together, these cross sections provide a composite picture of the nature and timing of environmental change across this part of the estuary from its initial flooding ~10 ka to its continued evolution by ~ 6 ka. A cross section analysis of the cores across the incised valley combined with interpolated ages from the age models shows consistent paleoenvironmental changes across multiple cores (Figure 15). PC-2 and PC-4 do not transition from upper bay to central bay environments at the same time, likely due to the elevation of the Pleistocene terrace at PC-4's location. However, PC-2, PC-4, and GC-6 all transition from central bay to outer bay environments at approximately the same time – 8.2-8.0 ka. Shortly after this change, GC-4 transitions to an outer bay environment at ~7.9 ka, and outer bay sediments thicken in the cores moving seaward from PC-2. Similarly, GC-2 and GC-5 show a coincident transition to outer bay environment at ~8.4 ka (Figure 15).

Additionally, all cores in the study area, except for GC-6, appear to transition to an inner shelf environment by ~6.0 ka, although this interval is difficult to date because of the likely erosion of material during transgression and the limited upper seafloor sediments observed in all cores (Figure 16). This coincident timing suggests that the paleoestuary was stable and changes in shoreline position and/or lateral shifts in the position of the tidal inlet led to the observed environmental transitions. Overall, the lateral differences in sediments within the cores reflect contemporaneous estuarine environmental variability.

Micropaleontologic evidence from these cores confirm the existence of a long-term stable estuarine environment; however, the seaward boundary of this estuary differs from previous studies (Figure 17). Approximately 9.8-9.6 ka, a large estuary stretched from the modern shoreline of Galveston Bay to seaward of Heald Bank. The flood-tidal delta at the base of GC-2 combined with the 8.7 ka age of the transgressive ravinement identified by Thomas and Anderson (1994) indicates the shoreline shifted landward of Heald Bank by at least 8.8 ka. This finding is inconsistent with the interpretation by Rodriguez et al. (2004) that the paleoestuary extended to seaward of Heald Bank until 7.7 ka. Our data indicate the paleoestuary was stable landward of Heald Bank for ~2 kyr with some tidal inlet changes that altered the environment within the estuary without transgressing the shoreline (Figure 17). A subsequent landward shift took place ~6.9 ka when the barrier system transgressed to a location between GC-2 and GC-5. By ~6.0 ka the locations of almost all cores in the study area transitioned to inner shelf environments. Washover deposits in GC-6 combined with inner shelf environment of the cores, indicate the shoreline was landward of the study area, but did not reach its modern location until

~2.5 ka when Bolivar Peninsula began to prograde calling into question the interpretation of Galveston Island forming as early as 5.3 ka (Rodriguez et al., 2004).

5.1 *Stable paleoestuary*

Research conducted by the Anderson group argues for the existence of >75 km long paleoestuary from Heald Bank ~50 km offshore Galveston Bay to the modern bay between ~8.2-7.8 ka (Figure 1) (Anderson et al., 2008; Rodriguez et al., 2004). This evidence includes seismic data and carbon dating of sediment cores from within modern Galveston Bay and Heald Bank (Anderson et al., 2008; Rodriguez et al., 2004).

Our data support the long-term stability of the estuary system during this interval, but not the extension of the estuary all the way to Heald Bank. Foraminiferal analysis from PC-2 and PC-4 indicates that both sites were located in the central bay from at least 8.8 ka to 8.0 ka, although PC-2 transitioned to a central bay environment by ~9.6 ka, confirming the existence of a long-term stable estuary (Figures 7 & 8). Foraminiferal assemblages in PC-2 and PC-4 during this time period were dominated by *Ammonia* with a secondary presence of *Elphidium*, corresponding to a central bay depositional environment. Assemblages in PC-4 moving up through the core show a decreasing abundance of *Ammonia* and an increase in *Elphidium* over time indicating a gradual environmental transition from upper bay to central bay and to outer bay. However, higher resolution analysis of PC-2 shows fluctuations in *Ammonia* and *Elphidium* abundances throughout the entire central bay interval, which may correspond to salinity fluctuations within the Holocene estuary as tidal inlets changed shape and/or location, or perhaps as precipitation in the catchment varied. Additionally, many of the peaks in *Ammonia* correspond to small increases in foram fragmentation, which may indicate reworking of central bay material during that interval. The PC-2 analysis indicates that portions of the estuary experienced marine mixing ~8.4 ka coinciding with a transition of seaward core locations to outer bay environments. Increased marine influence on the estuary may provide an explanation for the small variations in foraminiferal assemblages observed in the middle estuary.

GC-4 is located at the western edge of the paleovalley and contains sediment and foraminiferal assemblages that record lateral variation in the boundary of the estuary between ~8.2 ka and ~8.1 ka (Figure 11 and 15). While it is difficult to pinpoint the exact forcing mechanism for this expansion with existing evidence, the coincident timing of this flooding of boundaries and the environmental transition in GC-6 show that the outer western boundary of the paleoestuary flooded due to sea-level rise prior to probable partial barrier collapse and the transition to an outer bay seen first in GC-6 and subsequently in PC-2 and PC-4 (Figure 15). Although this flooding may have impacted the stability of the barrier system, it is unlikely that the shoreline changed significantly because GC-2 maintained an outer bay environment during this time (Figure 14), as well as the existence of tidal delta deposits identified by Thomas and Anderson (1994) (Figure 17). However, this hypothesis would require further analysis of high-resolution seismic data as well as additional coring and carbon dating to constrain the extent of the paleoestuary flooding.

5.2 *Paleoshoreline changes*

Rodriguez et al. (2004) describe estuarine muds in Heald Bank cores that were dated to 8,015 ± 50 and 7,770 ± 65 yr ago and suggested that the outer boundary of the paleoestuary was seaward of Heald Bank until ~7.77 ka. Due to the lack of preservation of barrier islands offshore in the sediment record, we must infer original island locations or areas of development based on the data that are preserved. Tidal inlet and tidal delta deposits are considered evidence for the presence of barrier systems that are not preserved (Anderson et al., 2016). Analysis of GC-2 reveals the existence of flood tide delta deposits dated to before ~8.5 ka, indicating that the inlet (and thus the barrier island system) was nearby and well landward of Heald Bank (Figure 14). Likewise, the presence of washover deposits in GC-5 at ~6.7 ka and GC-6 at ~4.3 ka demonstrates the landward migration of the paleoshoreline as sea level continued to rise throughout the Holocene (Figure 17). Both GC-2 and GC-5 transition to outer bay environments by ~8.4 ka (Figures 12 & 14), indicating that the outer boundary of the estuary shifted prior to the transition to what Rodriguez et al. (2004) describe as shoreface deposits in Heald Bank cores. A microfossil analysis of Heald Bank cores would have confirmed if the “estuarine” sediments described by Rodriguez et al. (2004) originated in an estuarine environment.

An earlier interpretation by Thomas and Anderson (1994) inferred Heald Bank and other sandy deposits on the Texas shelf to be marine sand banks. Despite their morphological similarities to barrier islands, many modern marine sand banks are not the result of “in-place drowning of barriers” (Snedden and Dalrymple, 1999); rather, they are actively modified marine deposits overlying a transgressive ravinement surface that likely formed from remnant ebb-tidal delta deposits as the shoreline shifted landward (Figure 17) (Dyer and Huntley, 1999; Penland et al., 1988). Based on the seismic interpretation of Thomas and Anderson (1994), Heald Bank formed from re-worked marine sands above a transgressive ravinement formed by erosion of estuarine deposits. The locations of Thomas, Shepard, and Heald Banks coincide with seismic facies interpreted as flood-tidal delta deposits (Thomas and Anderson, 1994), but were more likely to be ebb-tidal delta sediments (Figure 17). These sand banks likely formed as sand ridges off of seafloor irregularities at an angle from the ebb-tidal deltas and were later detached as the ebb-tidal delta was transgressed, providing source material for the sand banks (e.g., Type 2 sand ridges, Dyer and Huntley, 1999). Afterwards, these deposits were continually reworked by coastal currents as modern marine sand banks.

Sandy deposits in the outer bay sequence of GC-5 are likely washover sediments from a proximal barrier island. The absence of these sands in the bay margin intervals of GC-4 indicate that these washovers are not from the edge of the bay, westward of GC-5's location (Figure 12). We hypothesize that a barrier system developed near GC-5's position ~20 km seaward of the modern shoreline ~6.7 ka (Figure 17). Sandy intervals in the outer bay section of GC-2, located seaward of GC-5, dated to 6,973 ± 170 cal yr B.P. also suggest that a barrier had developed nearby in the distal direction, and these sandy intervals could represent paleo-storm washover deposits from that barrier system.

In addition to the data provided in GC-2 and GC-5, washover deposits in GC-6 (Figure 9) indicate that there was a barrier system proximal to GC-6's location between ~7.4 and 4.3 ka (Figure 17). The upper sample obtained from GC-6 closely resembles a modern marsh assemblage from Galveston Island (see 4.3), indicating that these washovers could be spilled over from either a back-barrier marsh or a marsh located on the edge of the paleoestuary, and are not a remnant ebb-tidal delta deposit (Figure 10).

Analysis of Galveston Island core data by Rodriguez et al. (2004) coupled with previous research on the island by Berrard et al. (1970) indicate that Galveston Island began prograding ~5.3 ka giving the paleoshoreline an irregular shape and showing rapid, rather than gradual, coastline changes in the past (Figure 1). Although Rodriguez et al. (2004) obtained their own radiocarbon ages, they indicated there was a significant amount of uncertainty in the methods used by Berrard et al. (1970). Excluding the work done by Berrard et al. (1970) leaves a single carbon date obtained by Rodriguez et al. (2004) from older beach ridges on Galveston Island providing an age of ~5.3 ka; this age could come from reworked material. The irregular shape of these paleoshorelines (Figure 1) is likely not representative of coastal changes which would have adjusted to sea-level rise “dynamically while maintaining a characteristic geometry that is unique to a particular coast” (FitzGerald et al., 2008). Based on probable washover sediments reported here, this paleoshoreline likely stepped landward multiple times until reaching is modern-day location by ~2.5 ka and the ~5.3 ka age thus represents reworked sediments. However, the lack of data between our study area and the modern shoreline makes it difficult to constrain this migration beyond its proximity to GC-6 at ~4.3 ka.

5.3 *Timeline of sea-level rise*

A comparison of environmental changes in the paleoestuary and the record of Gulf of Mexico sea-level rise indicates that most of these transitions coincide with or occurred after periods of rapid increases in sea level (Figure 16). A majority of these changes took place when global sea level rise was greater than twice the modern rate (~15 mm yr^{-1}), although some environmental shifts transpired after global sea level rise slowed significantly, indicating other regional and local changes, such as climate, may have contributed to these transitions (Figure 16).

Following the retreat of ice from Noble Inlet and Hudson Strait ~9.1 ka (Jennings et al., 2015), PC-4 transitioned to a central bay environment. The early opening of the Tyrell Sea in North America (now called Hudson Bay) ~8.7 ka (Jennings et al., 2015) preceded the transitions in GC-2 and GC-5 from central to outer bay as well as a brief increase in diversity in PC-2 that may represent increased marine mixing. The rapid discharge of freshwater from North American glacial lakes, dubbed the "8.2 ka event" that resulted in short-term climate cooling (Cronin et al., 2007; Jennings et al., 2015; Törnqvist et al., 2004; Ullman et al., 2016) coincided with the flooding of the paleoestuary that expanded at least the western boundary visible in GC-4, and the environmental change in GC-6 from central bay to outer bay ~8.2 ka. Following the 8.2 ka event, there was a reduced rate of global sea-level rise (Lambeck et al., 2014). GC-4 resumed a bay margin environment shortly afterwards, around the same time that PC-2 and PC-4 transitioned to outer bay (~8.1 ka). Glacial ice retreat in the Foxe Basin west of Baffin Island ~7.4 ka (Jennings et al., 2015) preceded a brief increase in diversity that we observe in GC-5, possibly associated with increased marine mixing due to an unstable barrier system ~7.3 ka. This change also coincides with a regional climate transition from cool/wet to warm/dry (Figure 16) (Weight et al., 2011), which may have contributed to environmental change through decreased precipitation and thus decreased sediment supply to the paleoestuary. GC-2 transitioned from outer bay to inner shelf ~6.9 ka approximately at the same time as the final deglaciation of the LIS ~6.7 ka (Jennings et al., 2015; Ullman et al., 2016). From 6.7 ka until the onset of recent accelerated sea-level rise (~100-150 yr ago), there was a progressive decrease in the rate of global sea-level rise (Lambeck et al., 2014). During this period, our study area transitioned to an inner shelf environment as the previously stable estuary system rapidly shifted landward (Figure 16), suggesting that climate-driven sediment supply played a significant role in maintaining the stability of the early-middle Holocene estuary and its protective barrier system and a reduction in this sediment supply precipitated retreat. This finding suggests that modern climate warming coupled with human reduced riverine sediment flux may increase the vulnerability of Galveston Island and Bolivar Peninsula in maintaining the modern coastline amid accelerating sea-level rise. The timing of the middle Holocene inner shelf transition is difficult to identify due to the removal of material above the transgressive ravinement with the exception of a single carbon date of a transgressive shell lag in GC-6 constraining probable washover deposits to younger than 4.3 ka.

5.4 *Minimal modern seafloor sedimentation*

The transition to a modern inner shelf environment is difficult to determine due to the limited amount of modern seafloor material and likely erosion and reworking of upper sediments from the transgressive ravinement. Although it appears to have happened slightly earlier in GC-2, it is probable that the study area was an inner shelf environment by ~6.0 ka and the transgression occurred over the period between 7.0 and 6.0 ka. The limited shelf material in the upper areas of each core represent deposition of ~0.01 cm per year, so it is more likely that material is being removed from the upper seafloor regularly.

The Texas Mud Blanket (TMB) is a large (~300 km^3) depositional area on the western Gulf Coast between a bathymetric embayment of the ancient Rio Grande and Colorado River deltas containing ~$5x10^{11}$ t of sediment (Weight et al., 2011). Weight et al. (2011) approximated mass accumulation rates in the TMB for the Holocene, with highest accumulation occurring from ~9 ka to ~5.5 ka and ~3.5 ka to present. The primary sediment source for the 9-5.5 ka period corresponds to the erosion of nearby Brazos and Colorado deltas, and accumulation decreased as these sediment sources were depleted (Weight et al., 2011). The period of ~3.5 ka to present accounts for 57% of total volume accumulation in the TMB, which is attributed to increased efficiency of marine longshore current, specifically the Louisiana-Texas Coastal Current, bringing sediments from as far as the Mississippi River delta (Weight et al., 2011). It is likely that the same mechanism has depleted inner shelf sediments offshore Galveston Bay resulting in minimal modern seafloor sediments in our cores with sediment delivered to regions farther west along the Texas Coast including the TMB.

6. Conclusion

We revise the established Holocene coastal change model for the Trinity River incised valley based on new radiocarbon dates and micropaleontological analysis of sediment cores from offshore Galveston Bay, Texas. This study provides environmental context to previous research that primarily utilized seismic and sedimentological analyses revealing consistent environmental changes across multiple cores due to external sea-level rise and climate forcing. As a result of this analysis, we reached the following conclusions:

- The barrier system was inshore of the modern position of Heald Bank prior to 8.5 ka with landward migration occurring in steps of barrier collapse and stabilization resulting in limited disruption during estuarine environmental transitions. It is unlikely that the shoreline migrated asymmetrically as previously hypothesized, but rather stepped landward in a pattern that approximates the geometry of the modern shoreline.

- Heald Bank, along with other sand banks along the Texas coast, is likely a marine sand bank developed above the transgressive ravinement from re-worked material after the shoreline shifted prior to 8.5 ka. The development of this marine sand body possibly began in connection with ebb-tidal delta deposits and is not a remnant or drowned barrier island.
- The Holocene estuary was stable for approximately 2 kyr (~6.9-8.8 ka) during which time the environment experienced minor, but noticeable, perturbations likely due to lateral variations in tidal inlets or partial collapse of barrier systems.
- Probable washover sediments in multiple cores approximate the location of barrier islands as they migrated landward at ~7-6.7 ka and after ~4.3 ka. The lack of data between our study area and the modern shoreline precludes our ability to map the migration of the barrier system beyond these approximations.
- Environmental changes within the Holocene estuary coincide with or follow glacial meltwater events from the LIS, with a majority of changes in the estuary occurring during the phase of more accelerated sea level rise in the early Holocene. As the rate sea level rise began to slow due to the final deglaciation of the LIS, additional probable regional hydroclimate forcing affecting the sediment supply resulted in continued environmental change shifting the estuary landward to its modern location.
- All cores in the study area contain minimal modern seafloor sediments likely due to erosion from the transgressive ravinement and re-working of sediment from ocean currents contributing to the Texas Mud Blanket.

7. Data Availability

Datasets related to this article can be found at XXX, an open-source online data repository hosted at YYYY (CITATION).

8. Acknowledgments

This project was funded by the Bureau of Ocean Energy Management under Cooperative Agreement M16AC00020, and the Martin B. Lagoe Micropaleontology Fellowship from the Jackson School of Geosciences at the University of the Texas at Austin. We would like to thank Gabriela Gutierrez, Daniel Duncan, Marcy Davis, the crew of the R/V *Brooks McCall*, TDI Brooks, the class of the 2018 Marine Geology and Geophysics Field Course, and the crew of the R/V *Manta* for their collective assistance in collecting the piston and gravity cores and additional chirp data for this study. We would also like to thank the National Ocean Sciences Accelerator Mass Spectrometry at Woods Hole Oceanographic Institute (NSF Cooperative Agreement number OCE-0753487) for processing our radiocarbon samples, and the Gulf of Mexico Sedimentology Working Group for discussions contributing to the analysis presented in this paper. We acknowledge that research on this project was conducted on land originally belonging to the Tonkawa Tribe before they were forcefully relocated to their current reservation land in Oklahoma in 1884 (http://www.tonkawatribe.com/). For more information about ancestral land you occupy, please visit https://native-land.ca/. This is University of Texas Institute for Geophysics Contribution #XXXX.

9. References

Abdulah, K.C., Anderson, J.B., Snow, J.N., Holdford-Jack, L., 2004. The Late Quaternary Brazos and Colorado Deltas, Offshore Texas, U.S.A.—Their Evolution and the Factors that Controlled Their Deposition.

Al Mukaimi, M.E., Dellapenna, T.M., Williams, J.R., 2018. Enhanced land subsidence in Galveston Bay, Texas: Interaction between sediment accumulation rates and relative sea level rise. Estuar. Coast. Shelf Sci. 207, 183–193. https://doi.org/10.1016/j.ecss.2018.03.023

Anderson, J.B., Rodriguez, A.B., Milliken, K.T., Taviani, M., 2008. The Holocene evolution of the Galveston estuary complex, Texas: Evidence for rapid change in estuarine environments, in: Special Paper 443: Response of Upper Gulf Coast Estuaries to Holocene Climate Change and Sea-Level Rise. Geological Society of America, pp. 89–104. https://doi.org/10.1130/2008.2443(06)

Anderson, J.B., Wallace, D.J., Simms, A.R., Rodriguez, A.B., Milliken, K.T., 2014. Variable response of coastal environments of the northwestern Gulf of Mexico to sea-level rise and climate change: Implications for future change. Mar. Geol. 352, 348–366.

Anderson, J.B., Wallace, D.J., Simms, A.R., Rodriguez, A.B., Weight, R.W.R., Taha, Z.P., 2016. Recycling sediments between sourece and sink during a eustatic cycle: Systems of late Quaternary northwestern Gulf of Mexico Basin. Earth-Sci. Rev. 153, 111–138.

Bamber, J.L., Oppenheimer, M., Kopp, R.E., Aspinall, W.P., Cooke, R.M., 2019. Ice sheet contributions to future sea-level rise from structured expert judgment. Proc. Natl. Acad. Sci. 116, 11195–11200. https://doi.org/10.1073/pnas.1817205116

Bernstein, A., Gustafson, M.T., Lewis, R., 2019. Disaster on the horizon: The price effect of sea level rise. J. Financ. Econ. 134, 253–272. https://doi.org/10.1016/j.jfineco.2019.03.013

Blaauw, M., Christen, J.A., 2011. Flexible paleoclimate age-depth models using an autoregressive gamma process. Bayesian Anal. 6, 457–474. https://doi.org/10.1214/11-BA618

Brenner, O.T., Moore, L.J., Murray, A.B., 2015. The complex influences of back-barrier deposition, substrate slope and underlying stratigraphy in barrier island response to sea-level rise: Insights from the Virginia Barrier Islands, Mid-Atlantic Bight, U.S.A. Geomorphology 246, 334–350. https://doi.org/10.1016/j.geomorph.2015.06.014

Burstein, J., Goff, J.A., Gulick, S., Lowery, C., Standring, P., Swartz, J., 2021. Tracking Barrier Island Response to Early Holocene Sea-level Rise: High Resolution Study of Estuarine Sediments in the Trinity River Paleovalley.

Buzas, M.A., 1990. Another look at confidence limits for species proportions. J. Paleontol. 2.

Cronin, T.M., Vogt, P.R., Willard, D.A., Thunell, R., Halka, J., Berke, M., Pohlman, J., 2007. Rapid sea level rise and ice sheet response to 8,200-year climate event. Geophys. Res. Lett. 34. https://doi.org/10.1029/2007GL031318

Culver, S.J., 1988. New Foraminiferal Depth Zonation of the Northwestern Gulf of Mexico. PALAIOS 3, 69–85. https://doi.org/10.2307/3514545

Davis, R.A., Hayes, M.O., 1984. What is a wave-dominated coast? Mar. Geol., Hydrodynamics and Sedimentation in Wave-Dominated Coastal Environments 60, 313–329. https://doi.org/10.1016/0025-3227(84)90155-5

Dutton, A., Carlson, A.E., Long, A.J., Milne, G.A., Clark, P.U., DeConto, R., Horton, B.P., Rahmstorf, S., Raymo, M.E., 2015. Sea-level rise due to polar ice-sheet mass loss during past warm periods. Science 349. https://doi.org/10.1126/science.aaa4019

Dyer, K.R., Huntley, D.A., 1999. The origin, classification and modelling of sand banks and ridges. Cont. Shelf Res. 19, 1285–1330. https://doi.org/10.1016/S0278-4343(99)00028-X

FitzGerald, D.M., Fenster, M.S., Argow, B.A., Buynevich, I.V., 2008. Coastal Impacts Due to Sea-Level Rise. Annu. Rev. Earth Planet. Sci. 36, 601–647. https://doi.org/10.1146/annurev.earth.35.031306.140139

Fred B. Phleger, 1960. Sedimentary patterns of microfaunas in northern Gulf of Mexico 34, 267–301.

Fruergaard, M., Møller, I., Johannessen, P.N., Nielsen, L.H., Andersen, T.J., Nielsen, L., Sander, L., Pejrup, M., 2015. Stratigraphy, Evolution, and Controls of A Holocene Transgressive–Regressive Barrier Island Under Changing Sea Level: Danish North Sea Coast. J. Sediment. Res. 85, 820–844. https://doi.org/10.2110/jsr.2015.53

Gehrels, W.R., 2013. Microfossil-Based Reconstruction of Holocene Relative Sea-Level Change. Sea Level Stud.

Goff, J.A., Allison, M.A., Gulick, S.P.S., 2010. Offshore transport of sediment during cyclonic storms: Hurricane Ike (2008), Texas Gulf Coast, USA. Geology 38, 351–354. https://doi.org/10.1130/G30632.1

Goff, J.A., Flood, R.D., Austin, Jr., James A., Schwab, W.C., Christensen, B., Browne, C.M., Denny, J.F., Baldwin, W.E., 2015. The impact of Hurricane Sandy on the shoreface and inner shelf of Fire Island, New York: Large bedform migration but limited erosion. Cont. Shelf Res. 98, 13–25. https://doi.org/10.1016/j.csr.2015.03.001

Haslett, J., Parnell, A., 2008. A simple monotone process with application to radiocarbon-dated depth chronologies. J. R. Stat. Soc. Ser. C Appl. Stat. 57, 399–418. https://doi.org/10.1111/j.1467-9876.2008.00623.x

Hawkes, A.D., Horton, B.P., 2012. Sedimentary record of storm deposits from Hurricane Ike, Galveston and San Luis Islands, Texas. Geomorphology 171–172, 180–189. https://doi.org/10.1016/j.geomorph.2012.05.017

Heaton, T.J., Köhler, P., Butzin, M., Bard, E., Reimer, R.W., Austin, W.E.N., Ramsey, C.B., Grootes, P.M., Hughen, K.A., Kromer, B., Reimer, P.J., Adkins, J., Burke, A., Cook, M.S., Olsen, J., Skinner, L.C., 2020. Marine20—The Marine Radiocarbon Age Calibration Curve (0–55,000 cal BP). Radiocarbon 62, 779–820. https://doi.org/10.1017/RDC.2020.68

Horton, B.P., R.E. Kopp, A. Dutton, T.A. Shaw, 2019. Geological records of past sea-level changes as constraints for future projections. Past Glob. Chang. Mag. 27. https://doi.org/10.22498/pages.27.1.28

Jennings, A., Andrews, J., Pearce, C., Wilson, L., Ólfasdótttir, S., 2015. Detrital carbonate peaks on the Labrador shelf, a 13–7ka template for freshwater forcing from the Hudson Strait outlet of the Laurentide Ice Sheet into the subpolar gyre. Quat. Sci. Rev. 107, 62–80. https://doi.org/10.1016/j.quascirev.2014.10.022

Kirwan, M.L., Megonigal, J.P., 2013. Tidal wetland stability in the face of human impacts and sea-level rise. Nature 504, 53–60. https://doi.org/10.1038/nature12856

K.T. Milliken, J.B. Anderson, A.B. Rodriguez, 2008. A new composite Holocene sea-level curve for the northern Gulf of Mexico., in: Response of Upper Gulf Coast Estuaries to Holocene Climate Change and Sea Level Rise, Geological Society of America Special Paper 443. pp. 1–11.

Lambeck, K., Rouby, H., Purcell, A., Sun, Y., Sambridge, M., 2014. Sea level and global ice volumes from the Last Glacial Maximum to the Holocene. Proc. Natl. Acad. Sci. 111, 15296–15303. https://doi.org/10.1073/pnas.1411762111

Lentz, E.E., Hapke, C.J., Stockdon, H.F., Hehre, R.E., 2013. Improving understanding of near-term barrier island evolution through multi-decadal assessment of morphologic change. Mar. Geol. 337, 125–139. https://doi.org/10.1016/j.margeo.2013.02.004

Lorenzo-Trueba, J., Ashton, A.D., 2014. Rollover, drowning, and discontinuous retreat: Distinct modes of barrier response to sea-level rise arising from a simple morphodynamic model. J. Geophys. Res. Earth Surf. 119, 779–801. https://doi.org/10.1002/2013JF002941

Miller, M.M., Shirzaei, M., 2021. Assessment of Future Flood Hazards for Southeastern Texas: Synthesizing Subsidence, Sea-Level Rise, and Storm Surge Scenarios. Geophys. Res. Lett. 48, e2021GL092544. https://doi.org/10.1029/2021GL092544

Moore, L.J., List, J.H., Williams, S.J., Stolper, D., 2010. Complexities in barrier island response to sea level rise: Insights from numerical model experiments, North Carolina Outer Banks. J. Geophys. Res. Earth Surf. 115. https://doi.org/10.1029/2009JF001299

Olson, H.C., Leckie, R.M. (Eds.), 2003. Micropaleontologic Proxies for Sea-Level Change and Stratigraphic Discontinuities. SEPM (Society for Sedimentary Geology). https://doi.org/10.2110/pec.03.75

Paine, J.G., 1993. Subsidence of the Texas coast: inferences from historical and late Pleistocene sea levels. Tectonophysics, Geological Perspetives on Global Change 222, 445–458. https://doi.org/10.1016/0040-1951(93)90363-O

Palermo, R.V., Piliouras, A., Swanson, T.E., Ashton, A.D., Mohrig, D., 2021. The effects of storms and a transient sandy veneer on the interannual planform evolution a low-relief coastal cliff and wave-cut platform at Sargent Beach, Texas, USA. Earth Surf. Dyn. Discuss. 1–20.

Penland, S., Boyd, R., Suter, J.R., 1988. Transgressive depositional systems of the Mississippi Delta plain; a model for barrier shoreline and shelf sand development. J. Sediment. Res. 58, 932–949. https://doi.org/10.1306/212F8EC2-2B24-11D7-8648000102C1865D

Phillips, J.D., Slattery, M.C., Musselman, Z.A., 2004. Dam-to-delta sediment inputs and storage in the lower trinity river, Texas. Geomorphology 62, 17–34. https://doi.org/10.1016/j.geomorph.2004.02.004

Phleger, F.B., 1965. Patterns of Marsh Foraminifera, Galveston Bay, Texas. Limnol. Oceanogr. 10, R169–R184. https://doi.org/10.4319/lo.1965.10.suppl2.r169

Phleger, F.B., 1951. Ecology of Foraminifera, Northwest Gulf of Mexico. Geological Society of America.

Poag, C.W., 1981. Benthic Foraminifera of the Gulf of Mexico.

Raff, J.L., Shawler, J.L., Ciarletta, D.J., Hein, E.A., Lorenzo-Trueba, J., Hein, C.J., 2018. Insights into barrier-island stability derived from transgressive/regressive state changes of Parramore Island, Virginia. Mar. Geol. 403, 1–19. https://doi.org/10.1016/j.margeo.2018.04.007

Ramsey, C.B., 2009. Bayesian Analysis of Radiocarbon Dates. Radiocarbon 51, 337–360. https://doi.org/10.1017/S0033822200033865

Rehkemper, L.J., 1969. Sedimentology of Holocene Estuarine Deposits, Galveston Bay 12–52.

Reimer, P.J., Austin, W.E.N., Bard, E., Bayliss, A., Blackwell, P.G., Ramsey, C.B., Butzin, M., Cheng, H., Edwards, R.L., Friedrich, M., Grootes, P.M., Guilderson, T.P., Hajdas, I., Heaton, T.J., Hogg, A.G., Hughen, K.A., Kromer, B., Manning, S.W., Muscheler, R., Palmer, J.G., Pearson, C., Plicht, J. van der, Reimer, R.W., Richards, D.A., Scott, E.M., Southon, J.R., Turney, C.S.M., Wacker, L., Adolphi, F., Büntgen, U., Capano, M., Fahrni, S.M., Fogtmann-Schulz, A., Friedrich, R., Köhler, P., Kudsk, S., Miyake, F., Olsen, J., Reinig, F., Sakamoto, M., Sookdeo, A., Talamo, S., 2020. The IntCal20 Northern Hemisphere Radiocarbon Age Calibration Curve (0–55 cal kBP). Radiocarbon 62, 725–757. https://doi.org/10.1017/RDC.2020.41

Rodriguez, A.B., Anderson, J.B., Simms, A.R., 2005. Terrace Inundation as an Autocyclic Mechanism for Parasequence Formation: Galveston Estuary, Texas, U.S.A. J. Sediment. Res. 75, 608–620. https://doi.org/10.2110/jsr.2005.050

Rodriguez, A.B., Anderson, J.B., Siringan, F.P., Taviani, M., 2004. Holocene Evolution of the East Texas Coast and Inner Continental Shelf: Along-Strike Variability in Coastal Retreat Rates. J. Sediment. Res. 74, 405–421. https://doi.org/10.1306/092403740405

Shawler, J.L., Ciarletta, D.J., Connell, J.E., Boggs, B.Q., Lorenzo-Trueba, J., Hein, C.J., 2021. Relative influence of antecedent topography and sea-level rise on barrier-island migration. Sedimentology 68, 639–669. https://doi.org/10.1111/sed.12798

Simms, A.R., Lambeck, K., Purcell, A., Anderson, J.B., Rodriguez, A.B., 2007. Sea-level history of the Gulf of Mexico since the Last Glacial Maximum with implications for the melting history for the Laurentide Ice Sheet. Quat. Sci. Rev. 26, 920–940.

Siringan, F.P., Anderson, J.B., 1993. Seismic facies, architecture, and evolution of the Bolivar Roads tidal inlet/delta complex, East Texas Gulf Coast. J. Sediment. Res. 63, 794–808. https://doi.org/10.1306/D4267C08-2B26-11D7-8648000102C1865D

Snedden, J.W., Dalrymple, R.W., 1999. Modern Shelf Sand Ridges: From Historical Perspective to a Unified Hydrodynamic and Evolutionary Model.

Swartz, J.M., 2019. Channel processes and products in subaerial and submarine environments across the Gulf of Mexico. University of Texas, Austin, Tex.

Thomas, M.A., Anderson, J.B., 1994. Sea-Level Controls on the Facies Architecture of the Trinity/Sabine Incised-Valley System, Texas Continental Shelf.
Törnqvist, T.E., Bick, S.J., González, J.L., Borg, K. van der, Jong, A.F.M. de, 2004. Tracking the sea-level signature of the 8.2 ka cooling event: New constraints from the Mississippi Delta. Geophys. Res. Lett. 31. https://doi.org/10.1029/2004GL021429
Ullman, D.J., Carlson, A.E., Hostetler, S.W., Clark, P.U., Cuzzone, J., Milne, G.A., Winsor, K., Caffee, M., 2016. Final Laurentide ice-sheet deglaciation and Holocene climate-sea level change. Quat. Sci. Rev. 152, 49–59. https://doi.org/10.1016/j.quascirev.2016.09.014
Vitousek, S., Barnard, P.L., Fletcher, C.H., Frazer, N., Erikson, L., Storlazzi, C.D., 2017. Doubling of coastal flooding frequency within decades due to sea-level rise. Sci. Rep. 7, 1399. https://doi.org/10.1038/s41598-017-01362-7
Wagner, A.J., Guilderson, T.P., Slowey, N.C., Cole, J.E., 2009. Pre-Bomb Surface Water Radiocarbon of the Gulf of Mexico and Caribbean as Recorded in Hermatypic Corals. Radiocarbon 51, 947–954. https://doi.org/10.1017/S0033822200034020
Wantland, K.F., 1969. Distribution of Modern Brackish-Water Foraminifera in Trinity Bay 93–117.
Weight, R.W.R., Anderson, J.B., Fernandez, R., 2011. Rapid Mud Accumulation On the Central Texas Shelf Linked To Climate Change and Sea-Level Rise. J. Sediment. Res. 81, 743–764. https://doi.org/10.2110/jsr.2011.57
White, W.A., Morton, R.A., Holmes, C.W., 2002. A comparison of factors controlling sedimentation rates and wetland loss in fluvial–deltaic systems, Texas Gulf coast. Geomorphology 44, 47–66. https://doi.org/10.1016/S0169-555X(01)00140-4

Tables

Table 1. List of radiocarbon dating samples and their calibrated ages.

No.	NOSAMS OS No.	Sample	Type	Process	Calibrated Age	
					Age (yr)	Error (± yr)
1	155814	PC-2-S3-7-8.5	Mollusc	Hydrolysis	7,441	127
2	152146	PC-2-S3-82-83.5	Mollusc	Hydrolysis	7,800	134
3	152138	PC-2-S2-69.5-71	Mollusc	Hydrolysis	8,468	135
4	152145	PC-2-S2-100.5-102	Mollusc	Hydrolysis	8,815	175
5	155815	PC-2-S1-14-16	Mollusc	Hydrolysis	9380	133
6	155816	PC-2-S1-23-25	Mollusc	Hydrolysis	9,420	124

7	155817	PC-2-S1-102-104	Mollusc	Hydrolysis	9,794	215
8	155818	PC-4-S3-58.5-60	Mollusc	Hydrolysis	7,787	136
9	152148	PC-4-S3-59	Mollusc	Hydrolysis	41,030	1,703
10	155819	PC-4-S2-15-16.5	Mollusc	Hydrolysis	8,815	175
11	152147	PC-4-S2-94-96	Mollusc	Hydrolysis	9,131	158
12	155820	GC-1-S1-4-6	Foraminifera	Hydrolysis	1,753	143
13	152314	GC-1-S1-5-6	Mollusc	Hydrolysis	589	97
14	152315	GC-1-S1-28.5-30	Foraminifera	Hydrolysis	38,081	1,833
15	155821	GC-2-S1-A-59-61	Mollusc	Hydrolysis	6,973	170
16	152310	GC-2-S2-144-145	Mollusc	Hydrolysis	8,445	135
17	152316	GC-2-S3-6-10	Mollusc	Hydrolysis	8,546	173
18	155902	GC-4-S1-55.5-56.5	Charcoal	Combustion	7,913	255
19	152149	GC-4-S2-13-13.5	Charcoal	Combustion	7,977	221
20	155903	GC-4-S3-120-122	Charcoal	Combustion	8,470	144
21	155822	GC-5-S2-3-5	Mollusc	Hydrolysis	6,661	169
22	155823	GC-5-S3-32-37.5	Mollusc	Hydrolysis	8,445	135
23	155824	GC-5-S3-74-76	Mollusc	Hydrolysis	8,467	130
24	155825	GC-6-S1-11-14	Mollusc	Hydrolysis	>Modern	
25	155826	GC-6-S1-64.5-66	Mollusc	Hydrolysis	4,329	165
26	157505	GC-6-S1-111.5-113	Mollusc	Hydrolysis	7,760	142
27	157506	GC-6-S1-130-131.5	Mollusc	Hydrolysis	7,709	147
28	157511	GC-6-S2-71-72.5	Mollusc	Hydrolysis	8,367	181

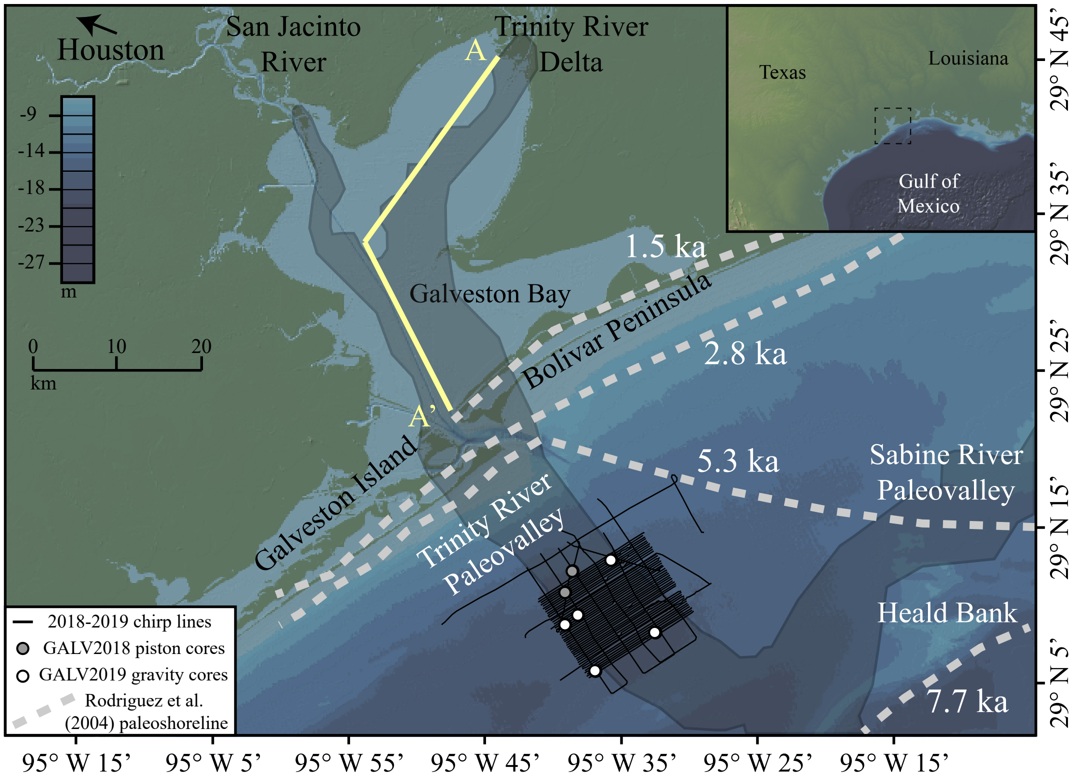

Figure 1. Study area offshore Galveston Bay, Texas, with Trinity River incised valley (gray outline), A-A' profile of cross-section shown in Figure 4 from Anderson et al. (2008), high-resolution seismic lines (black lines), 2018 piston cores (gray circles), 2019 gravity cores (white circles), and paleo-shorelines (gray dashed lines) based on interpretation from Rodriguez et al. (2004). Figure made with GeoMapApp (www.geomapapp.org) and Global Multi-Resolution Topography Data Synthesis (Ryan et al., 2009).

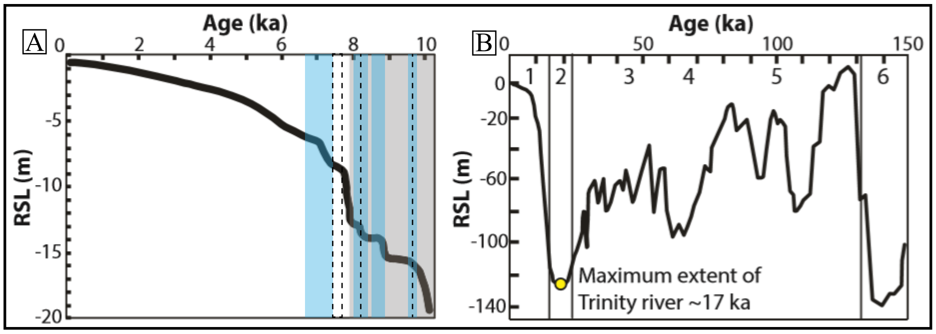

Figure 2. Holocene sea level curve. A) Sea level rise over the last 10 kyr with periods of rapid sea level rise identified by Milliken et al. (2008) (boxed in blue) and rapid sea level rise in Galveston Bay, Texas, identified by Anderson et al. (2008) (dashed lines). B) Holocene sea level curve over last 150 kyr showing Marine Isotope Stages 1-6 and maximum lowstand for the Trinity River occurring approximately 17 ka (modified from Swartz, 2019).

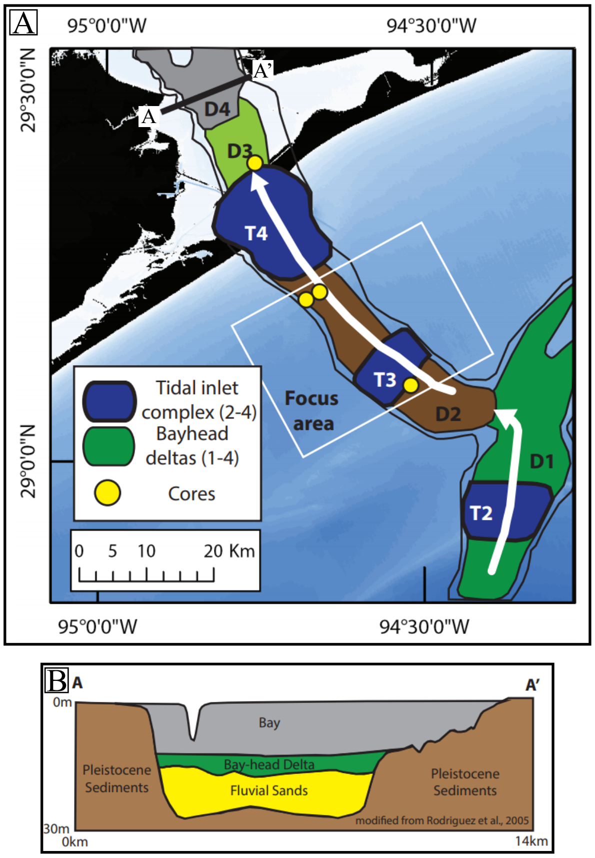

Figure 3. Trinity River transgressive systems tract. A) Landward changes of depositional facies due to Holocene sea level rise and study area offshore Galveston Bay, Texas. B) Cross-section of Trinity River Paleovalley within modern Galveston Bay, with generalized valley fill transitioning from fluvial sands to bay-head delta and bay fill deposits (modified from Swartz, 2019).

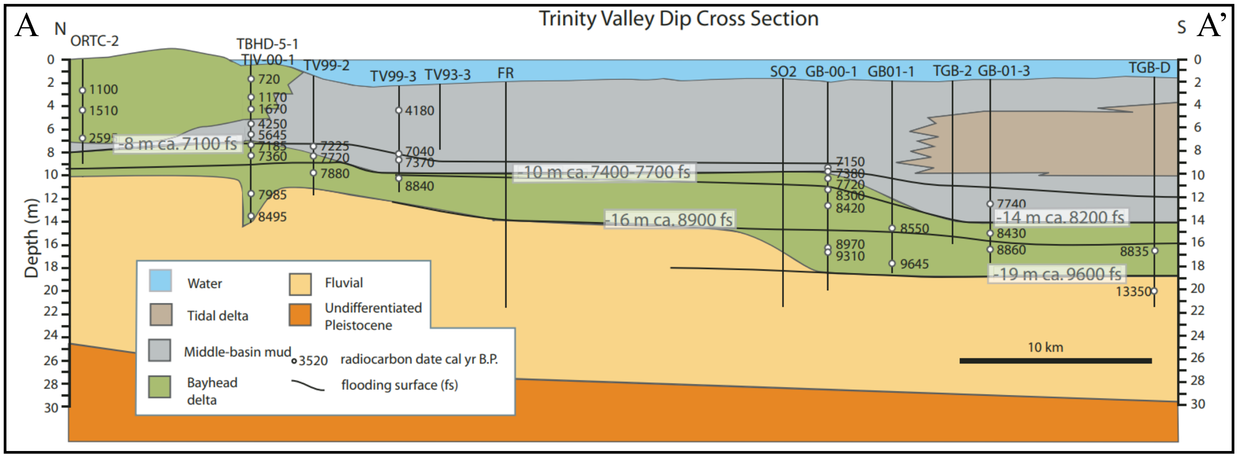

Figure 4. Cross section of the Trinity River Paleovalley in modern Galveston Bay, Texas (location in Figure 1), compiled from seismic and core data analyzed by Anderson Group displaying prominent sedimentary facies and flooding surfaces with radiocrabon ages (modified from Anderson et al., 2008).

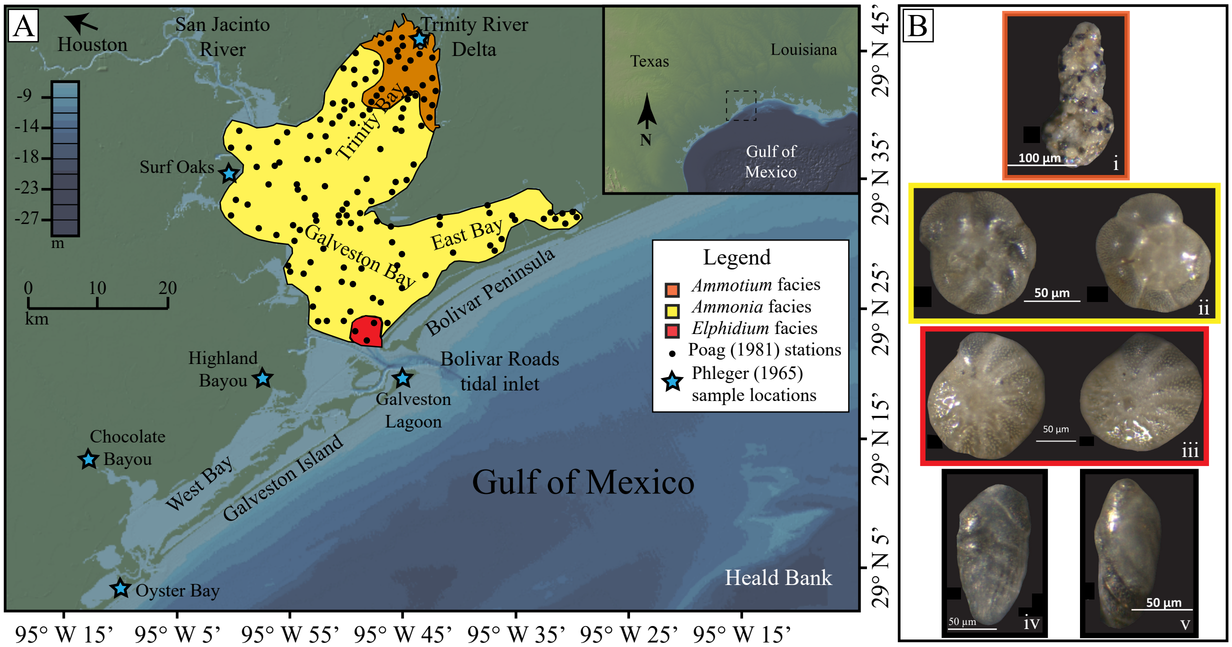

Figure 5. Foraminiferal predominance facies of Galveston Bay, Texas, based on Poag (1981). A) Map of Galveston Bay, Texas, showing areas within the modern estuary that are dominated by specific genera of foraminifera, and locations of marshes (blue stars) studied by Phleger (1965). B) Images of dominant genera of foraminifera: i) *Ammotium salsum* (orange; upper bay facies), ii) *Ammonia* sp. (yellow; central bay facies), iii) *Elphidium* sp. (red; outer bay facies), iv and v) *Bolivina* sp. and *Bulimina* sp., respectively, which are diagnostic genera for inner shelf facies (Culver, 1988) (modified from Poag, 1981, and Phleger, 1965). Figure made with GeoMapApp (www.geo-mapapp.org) and Global Multi-Resolution Topography Data Synthesis (Ryan et al., 2009).

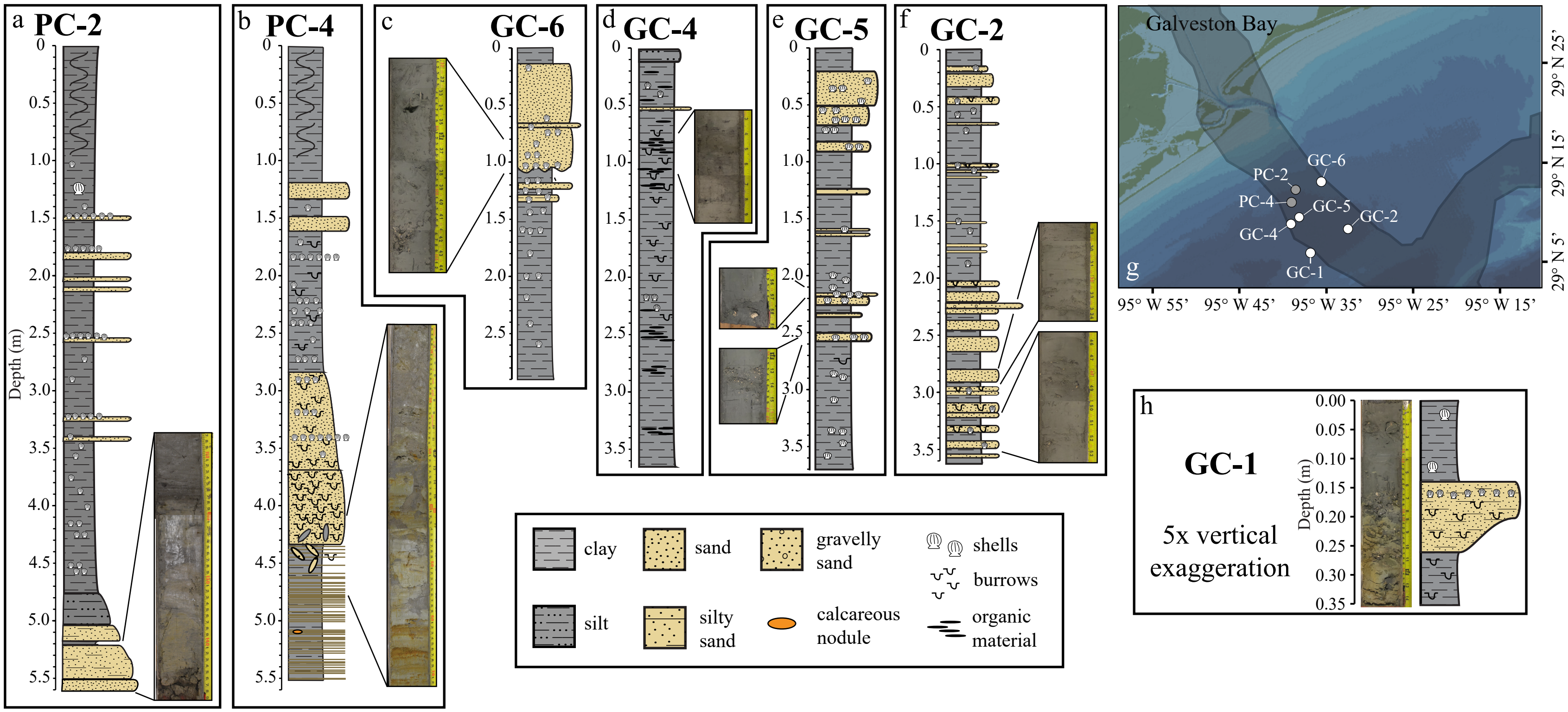

Figure 6. Stratigraphic columns and select core images from this study. a) PC-2 column with image of fluvial and upper bay sands (~5.2-5.6 m); b) PC-4 column with image of the Pleistocene terrace with oxidized sand in clay to upper bay heavily burrowed sands (~4.1-4.8 m); c) GC-6 column with image of outer bay shelly sands (0.8-1.1 m); d) GC-4 column with image of organic material (0.7-1.1 m); e) GC-5 column with images of large shells (2.1-2.2 m) and shell hash (2.5-2.6 m) in sandy sections; f) GC-2 column with images of sandy intervals containing shell fragments (2.8-2.9 m and 3.2-3.5 m); g) map of core locations offshore Galveston Bay; and h) GC-1 column and image of entire core (not at same scale as other cores).

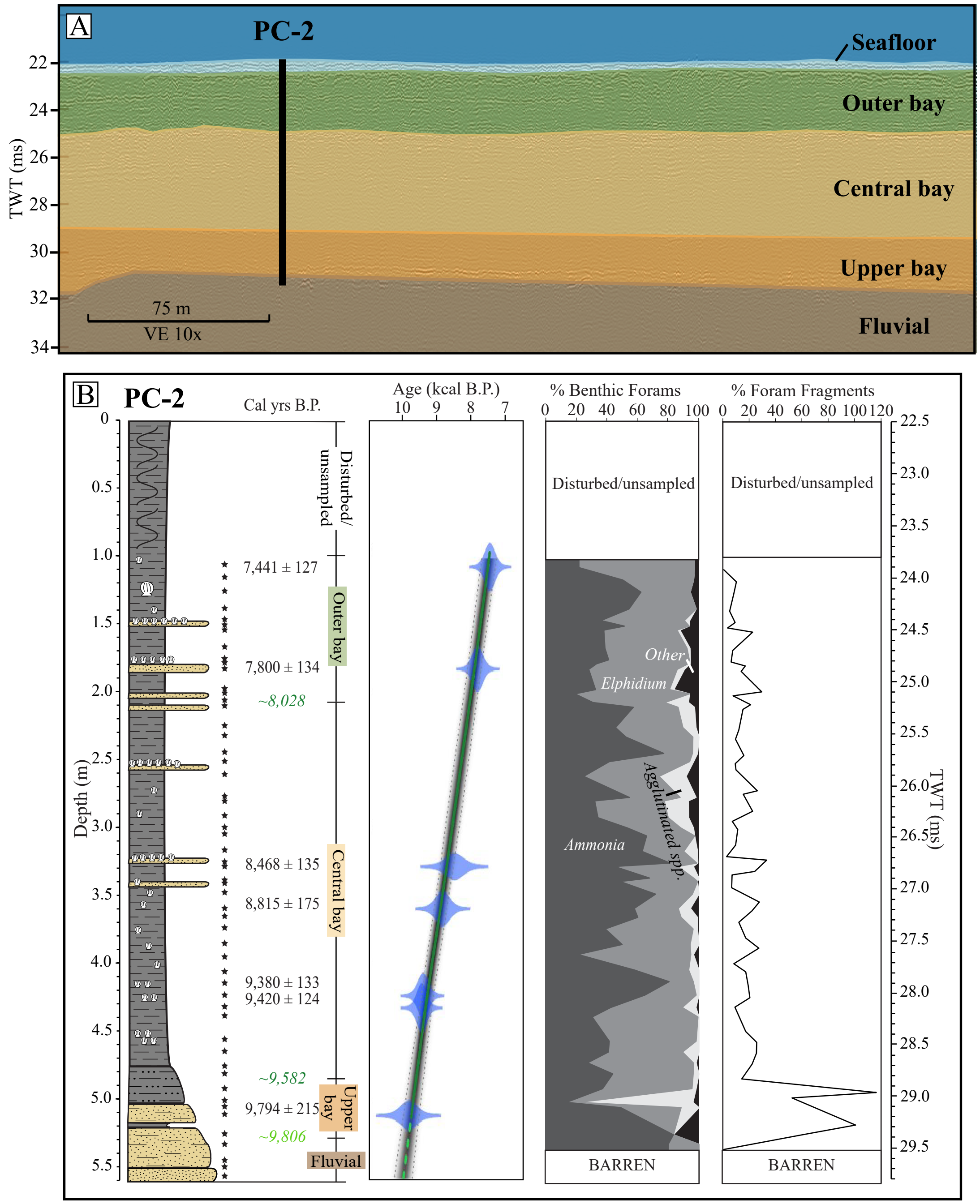

Figure 7. Piston Core 2 (PC-2). A) Interpreted seismic data with approximate depth of penetration for PC-2 (location in Figure 6). Seismic interpretation from Burstein et al. (in prep) (VE = vertical exaggeration). B) Stratigraphic column of PC-2 displaying sample locations (black stars), carbon dates (black), and interpolated and extrapolated ages (italicized in green) from age model. Age model based off of radiocarbon ages (blue ovals tapering to error range), with mean age depicted by solid dark green line for interpolated ages, light green dashed line for extrapolated ages, and gray scale out to 95% confidence interval predicted by the model. Interpreted depositional facies based off of foraminiferal assemblage abundances and percent foram fragments. Two-way travel time scale for stratigraphic column in ms calculated from approximate seismic velocity of 1,525 m/s starting at time of seafloor.

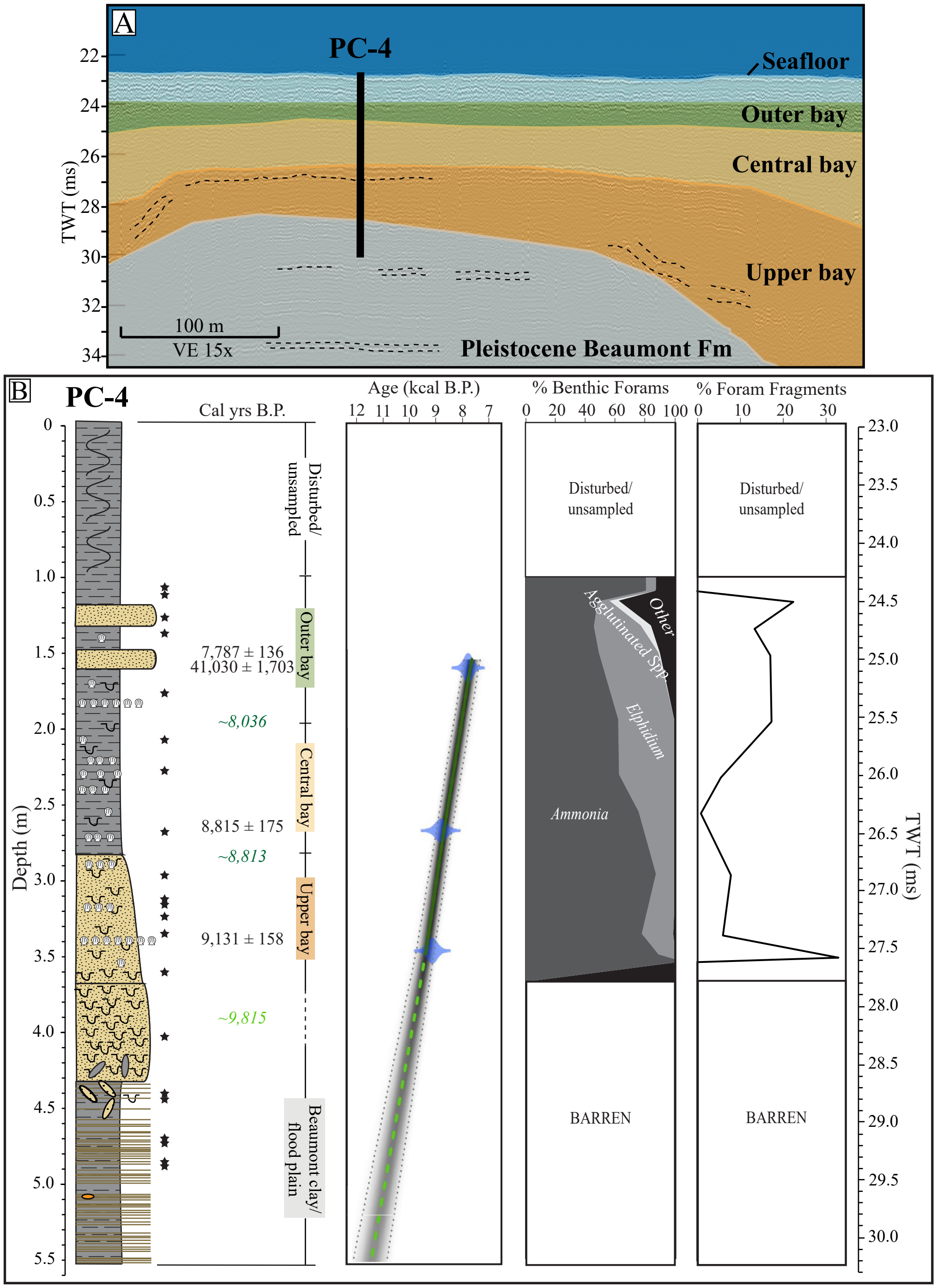

Figure 8. Piston Core 4 (PC-4). A) Interpreted seismic data with approximated depth for PC-4 into a Pleistocene terrace (location in Figure 6). Seismic interpretation from Burstein et al. (in prep) (VE = vertical exaggeration). B) Stratigraphic column with sample locations (black stars), carbon dates (black text), and interpolated and extrapolated ages (italicized in green) from age model. Age model based off of radiocarbon ages (blue ovals tapering to error range), with mean age depicted by dark green solid line for interpolated ages, light green dashed line for extrapolated ages, and gray scale out to 95% confidence interval predicted by the model. Interpreted depositional facies based off of foraminiferal assemblage abundances and percent foram fragments. Two-way travel time scale for stratigraphic column in ms calculated from approximate seismic velocity of 1,525 m/s starting at time of seafloor.

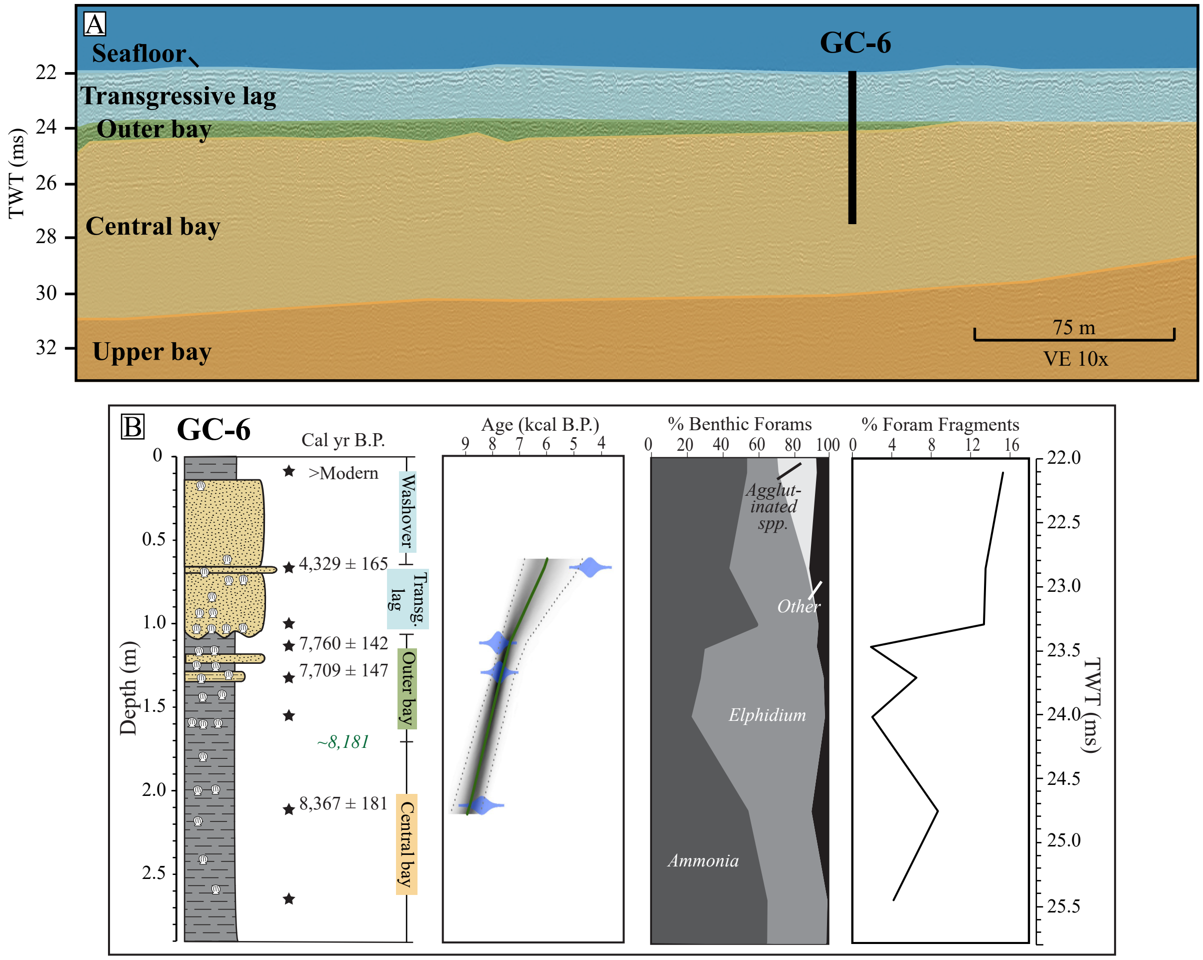

Figure 9. Gravity Core 6 (GC-6). A) Interpreted seismic data with approximate depth of penetration for GC-6 (location in Figure 6). Seismic interpretation from Burstein et al. (in prep) (VE = vertical exaggeration). B) Stratigraphic column with sample locations (black stars), radiocarbon dates (black text), interpolated ages (italicized in green) based off of age model. Age model based off of radiocarbon ages (blue ovals tapering to error range), with mean age depicted by solid green line and gray scale out to 95% confidence interval predicted by the model. Interpreted depositional facies based off of foraminiferal assemblage abundances and percent foram fragments. Two-way travel time scale for stratigraphic column in ms calculated from approximate seismic velocity of 1,525 m/s starting at time of seafloor.

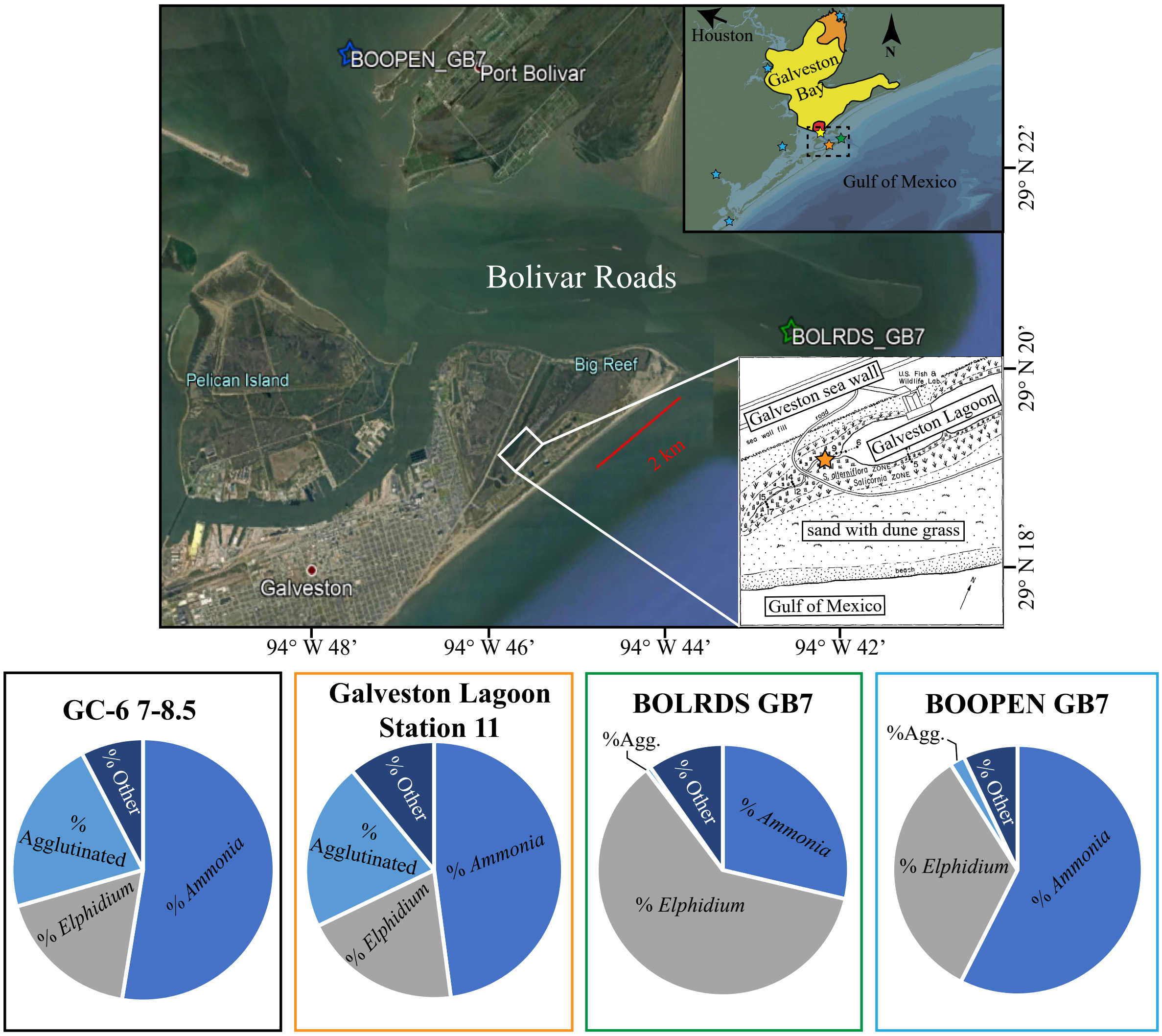

Figure 10. Comparison of GC-6 upper sample (7-8.5 cm) to modern foram assemblages: Galveston Lagoon sample from Station 11 analyzed by Phleger (1965) (orange), BOLRDS GB7 grab sample taken from the outer edge of the tidal inlet (green), and BOOPEN GB7 grab sample taken from the inner edge of the tidal inlet (blue). The Station 11 sample is the closest approximation to the GC-6 sample. Image source Google Earth (2021).

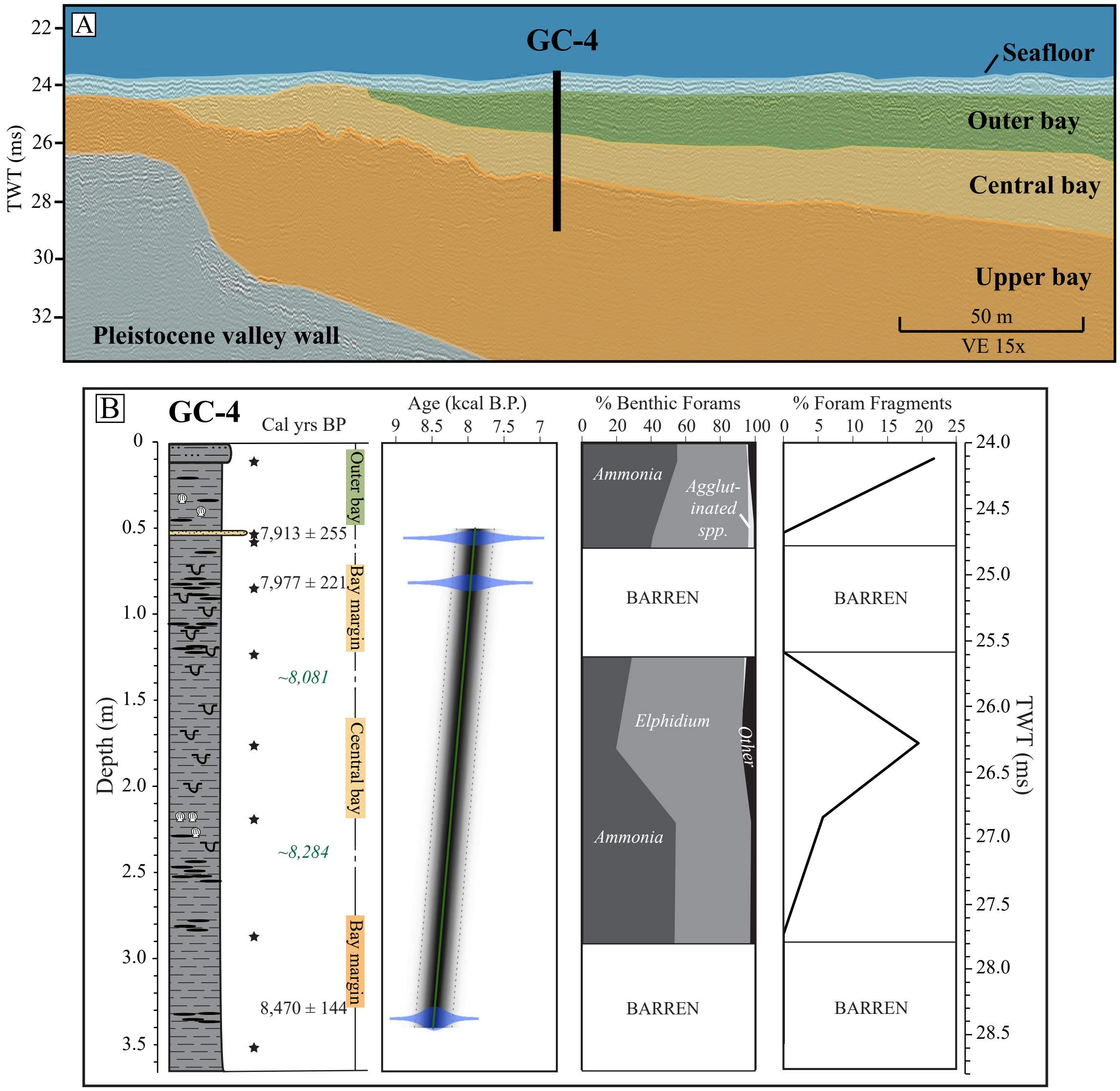

Figure 11. Gravity Core 4. A) Interpreted seismic data with approximate depth of penetration for GC-4 (location in Figure 6). Seismic interpretation from Burstein et al. (in prep) (VE = vertical exaggeration). B) Stratigraphic column of GC-4 showing samples (black stars) with radiocarbon ages (black text), interpolated ages (italicized in green) from age model. Age model based off of radiocarbon ages (blue ovals tapering to error range), with mean age depicted by solid green line and gray scale out to 95% confidence interval predicted by the model. Interpreted depositional facies based off of foraminiferal assemblage abundances and percent foram fragments. Two-way travel time scale for stratigraphic column in ms calculated from approximate seismic velocity of 1,525 m/s starting at time of seafloor.

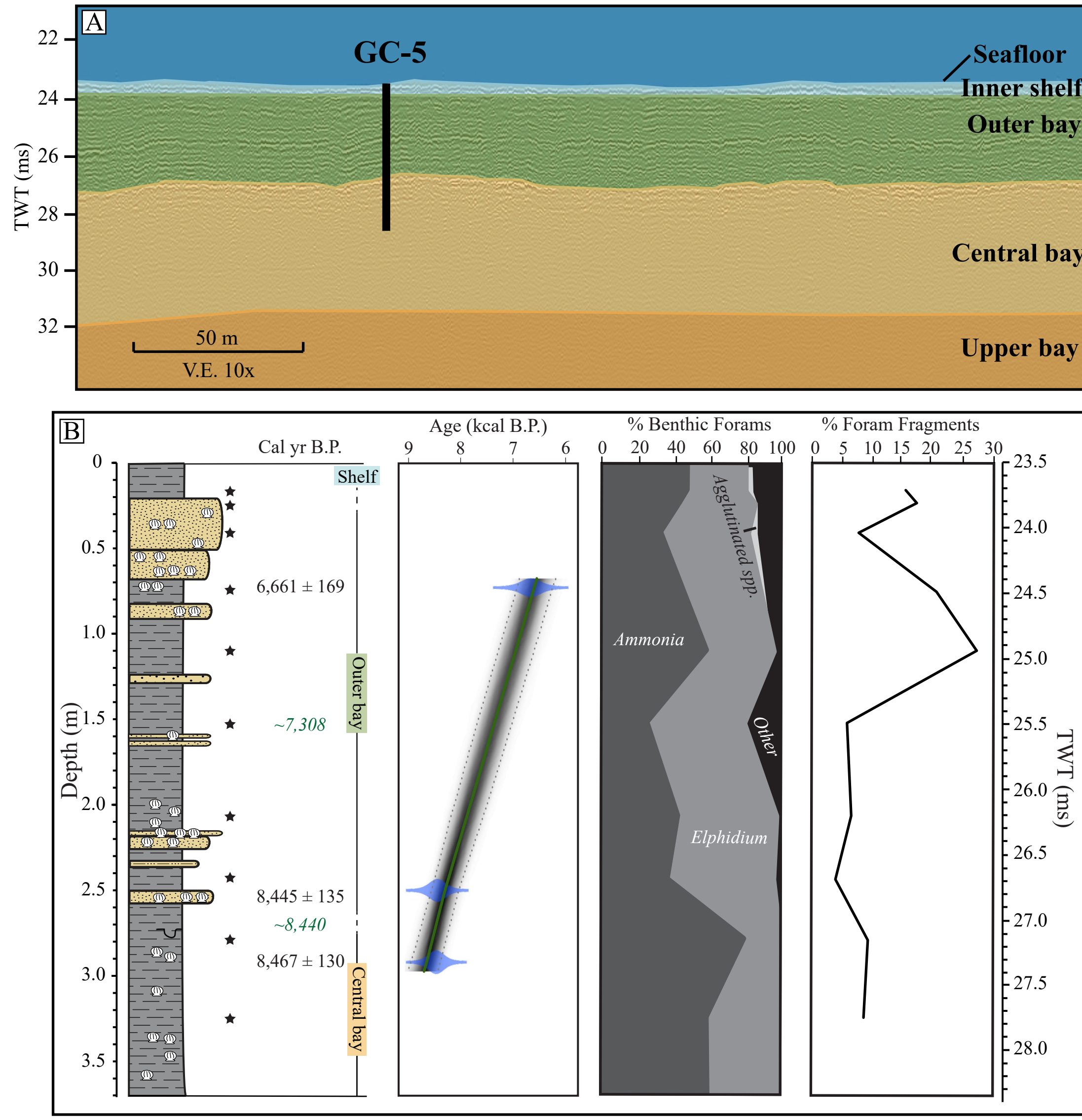

Figure 12. Gravity Core 5. A) Interpreted seismic data with approximate depth of penetration for GC-5 (location in Figure 6). Seismic interpretation from Burstein et al. (in prep) (VE = vertical exaggeration). B) Stratigraphic column of GC-5 showing samples (black stars) with radiocarbon ages (black text), interpolated ages (italicized in green) from age model. Age model based off of radiocarbon ages (blue ovals tapering to error range), with mean age depicted by solid green line and gray scale out to 95% confidence interval predicted by the model. Interpreted depositional facies based off of foraminiferal assemblage abundances and percent foram fragments. Two-way travel time scale for stratigraphic column in ms calculated from approximate seismic velocity of 1,525 m/s starting at time of seafloor.

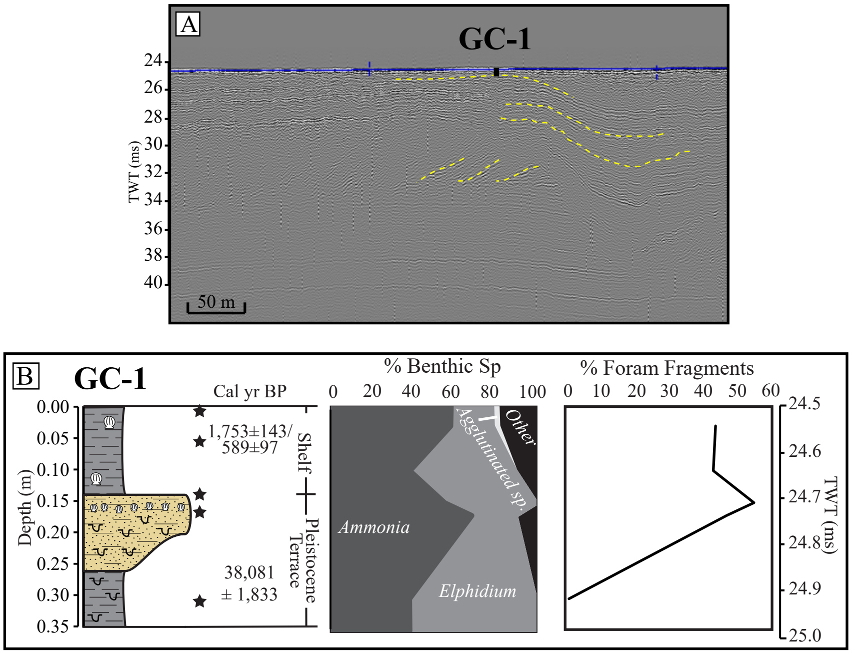

Figure 13. Gravity core 1 (GC-1). A) Uninterpreted seismic line showing location of GC-1 short core where it penetrated a high-elevation Pleistocene terrace. Yellow dashed lines show approximated interpretation of draped sediments and dipping reflectors. B) Stratigraphic column of GC-1 showing sample locations (black stars), radiocarbon dates, and interpreted depositional environments based on lithology, and foraminiferal assemblages and fragmentation. Two-way travel time (TWT) scale calculated based on approximate seismic velocity of 1,525 m/s starting at time of seafloor.

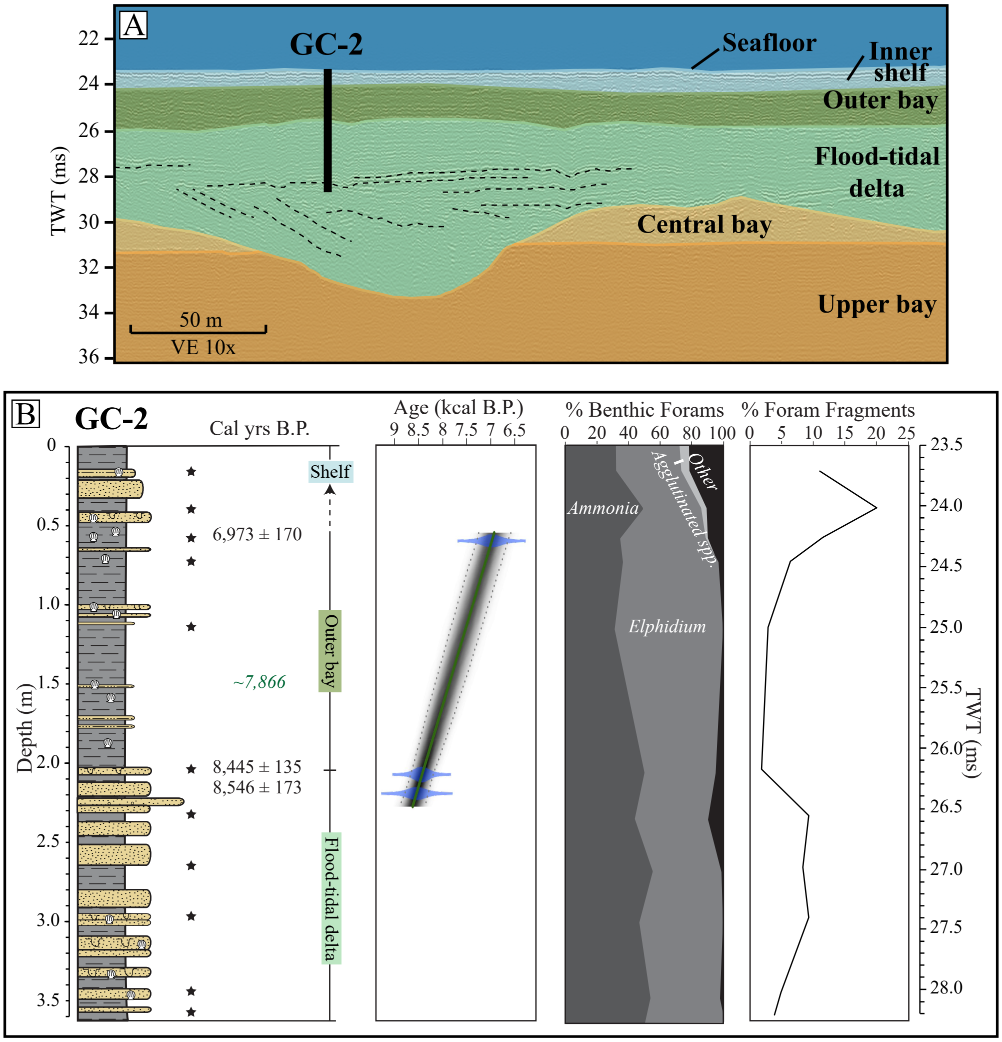

Figure 14. Gravity core 2 (GC-2). A) Interpreted seismic data with approximate depth of penetration for GC-2 (location in Figure 6). Seismic interpretation from Burstein et al. (in prep) (VE = vertical exaggeration). B) Stratigraphic column with sample locations (black stars), radiocarbon dates (black text), interpolated ages (italicized in green) from age model. Age model based off of radiocarbon ages (blue ovals tapering to error range), with mean age depicted by solid green line and gray scale out to 95% confidence interval predicted by the model. Interpreted depositional facies based off of foraminiferal assemblage abundances and percent foram fragments. Two-way travel time scale for stratigraphic column in ms calculated from approximate seismic velocity of 1,525 m/s starting at time of seafloor.

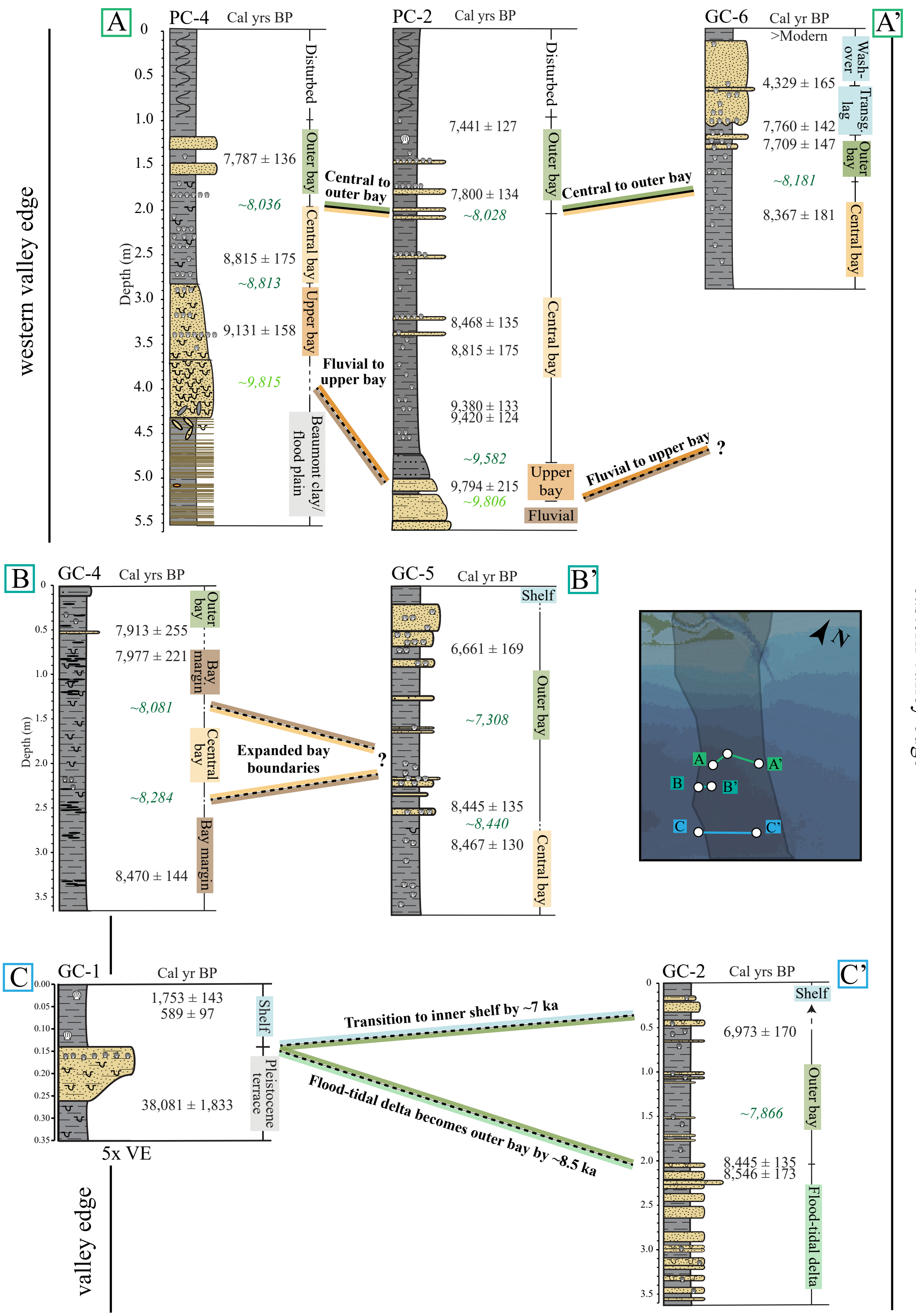

Figure 15. Fence diagram showing prominent environmental changes within cores within study area. Radiocarbon ages are in black text and interpolated and extrapolated ages from age model are italicized in green. Colored lines show connections between ages within cores along the profile.

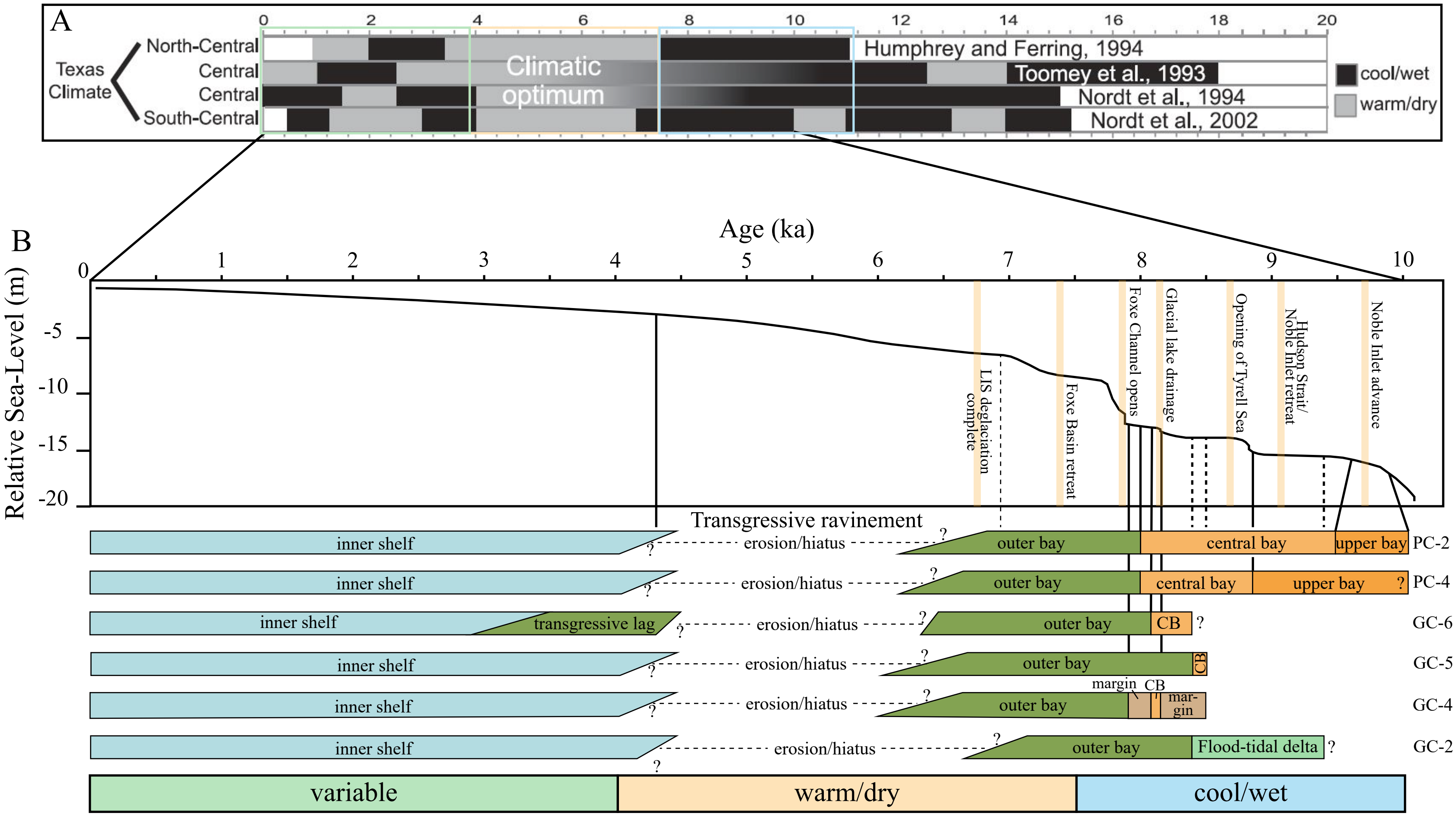

Figure 16. Timeline of environmental change and sea-level rise in Galveston paleostuary. A) Compilation of Gulf Coast climate for the Holocene (modified from Weight et al., 2011). B) Gulf Coast Holocene sea level curve containing prominent North American glacial events (beige lines) identified in Jennings et al. (2015) (modified from Swartz, 2019) and a compilation of environmental change within Trinity River paleovalley cores and approximated period of transgressive erosion. A majority of environmental transitions take place during a cool/wet climate when sea-level rise was more rapid, while significant transgressive erosion took place during a warm/dry period when sea-level rise slowed significantly.

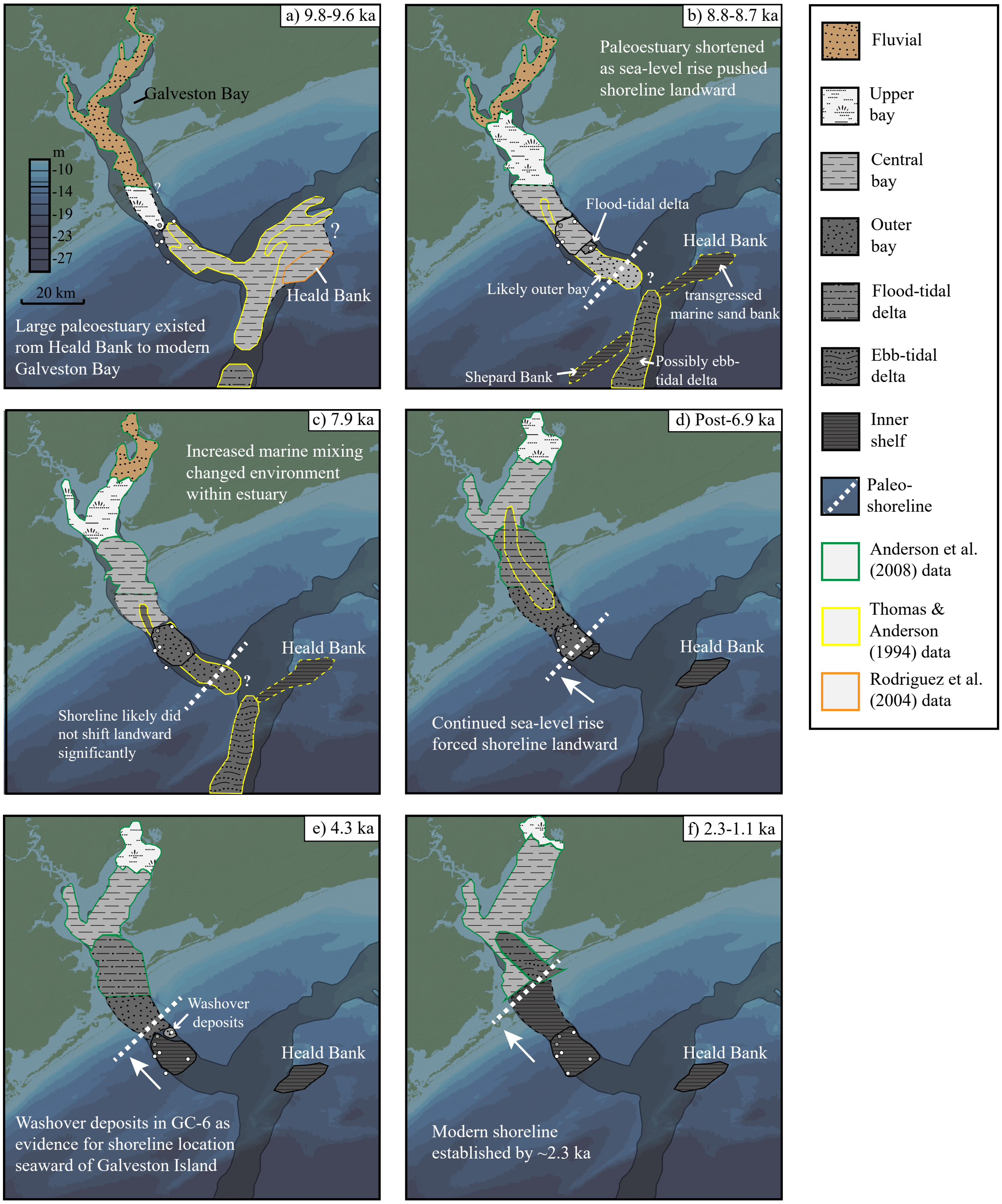

Figure 17. Summary of paleoenvironmental change of Holocene estuary offshore Galveston Bay, Texas. Environmental facies at specific periods of time are based on micropaleontological analysis of cores in study areas and combined with previous research (outlined in green, yellow, and orange), and inferences were made between these study areas (dashed outlines). Facies are mapped within the bounds of the incised valley, but likely extended beyond those boundaries; however, the outer boundaries are difficult to determine due to probable removal of sediments during marine transgression. Paleoshorelines are estimated based on proximity to tidal delta and outer bay environments, and identification of washover sediments in cores.